OPTIMIZATION OF POCKET MILLING TOOL PATH FOR CHATTER AVOIDANCE AND REDUCED MACHINING TIME

LUCY WANJA KARIUKI

MASTER OF SCIENCE

(Mechatronic Engineering)

JOMO KENYATTA UNIVERSITY OF

AGRICULTURE AND TECHNOLOGY

2017

Optimization of pocket milling tool path for chatter avoidance and reduced machining time

Lucy Wanja Kariuki

A thesis submitted in partial fulfillment for the degree of Master of Science in Mechatronic Engineering in the Jomo Kenyatta University of

Agriculture and Technology

2017

DECLARATION

This thesis is my original work and has not been presented for a degree in any other University.

Signature:..... Date.....

Lucy Wanja Kariuki

This thesis has been submitted for examination with our approval as the Univer-sity Supervisors.

Signature:..... Date.....

Prof. Eng. Benard W. Ikua, (PhD)

JKUAT, Kenya

Signature:..... Date.....

Prof. George N. Nyakoe, (PhD)

JKUAT, Kenya

DEDICATION

I dedicate this work to my parents, my husband Henry, and my sons Jayden and Manuel. Thank you for always believing in me.

ACKNOWLEDGEMENT

First and foremost, my gratitude goes to the Almighty God for enabling me to pursue this endevour. Secondly, I would like to acknowledge my supervisors, Prof. Eng. B. W. Ikua and Prof. G. N. Nyakoe for their invaluable guidance and advice throughout my studies.

I also wish to thank Jomo Kenyatta University of Agriculture and Technology for funding my studies. My appreciation also goes to the staff of Departments of Mechatronic Engineering and Mechanical Engineering for all their facilitation and assistance.

I acknowledge the administration and staff of National Youth Service(NYS) Engineering Institute for allowing me to use their machines and equipment to carry out my experiments.

Finally I wish to acknowledge my coursemates Brenda W. Nyota and Martin R. Maina, and all postgraduate students who walked this journey with me and offered invaluable input and criticism.

God bless you all.

TABLE OF CONTENTS

LIST OF FIGURES

LIST OF TABLES

LIST OF APPENDICES

NOMENCLATURE

$\boldsymbol{a}$	axial depth of cut
$\boldsymbol{A_c}$	chip area
$\boldsymbol{b}$	nominal depth of cut
$\boldsymbol{c}$	damping coefficient
$\boldsymbol{D}$	cutter diameter
$\boldsymbol{f}$	feedrate
$\boldsymbol{F_d}$	dynamic cutting force, N
$\boldsymbol{F_f}$	friction force, N
$\boldsymbol{F_n}$	normal force against friction, N
$\boldsymbol{F_s}$	static cutting force, N
$\boldsymbol{F_x}$	cutting force in x direction, N
$\boldsymbol{F_y}$	cutting force in y direction, N
$\boldsymbol{F_z}$	cutting force in z direction, N
$\boldsymbol{h}$	undeformed chip thickness
$\boldsymbol{h_c}$	chip thickness
$\boldsymbol{h_d}$	instantaneous dynamic chip thickness
$\boldsymbol{h_s}$	static chip thickness, mm
$\boldsymbol{k}$	stiffness constant
$\boldsymbol{K_{ac}}$	axial cutting coefficient
$\boldsymbol{K_{rc}}$	radial cutting/feed force coefficient
$\boldsymbol{K_{tc}}$	tangential cutting coefficient
$\boldsymbol{K_{ae}}$	axial edge coefficient
$\boldsymbol{K_{re}}$	radial edge coefficient
$\boldsymbol{K_{te}}$	tangential edge coefficient
$\boldsymbol{m}$	mass, g
$\boldsymbol{N}$	spindle speed, cycles per minute

n_t	number of teeth
r_c	chip thickness ratio
α_r	tool rake angle,
β	friction angle
γ	helix angle,
μ	coefficient of friction
ϕ	rotational angle
ϕ_{ex}	rotational angle at end of engagement
ϕ_{st}	rotational angle at start of engagement
ϕ_p	pitch angle,
ϕ_c	shear angle,
	lag angle
ρ	ratio of dynamic to static cutting force
τ_s	shear stress, N/mm^2

ABSTRACT

Modern Computer Numerical Control (CNC) machines and Computer Aided Manufacturing (CAM) systems have become quite sophisticated and can machine geometrically feasible pocket profiles. More than 80% of all mechanical parts which are manufactured by milling machines can be cut by Numerical Control (NC) pocket machining, which involves the removal of material within a closed boundary. Pocket milling is applied in the manufacture of dies and molds, and in the manufacture of aerospace and aircraft parts.

Most of the current Computer Aided Design and Computer Aided Manufacturing (CAD/CAM) systems used in CNC machines, such as Computer Aided Three-dimensional Interactive Application (CATIA) and Mastercam, provide the capability of generating NC pocket milling instructions based on the geometric definition of a workpiece and the cutter, thus automating part programming. However, the generation or selection of tool path is, in most cases, based on operator's experience and intuition. There is no consideration of the dynamic effects of the cutting process. This presents shortcomings that limit the productivity of a CNC machining system since the efficiency of the tool path strategy impacts on the overall efficiency of the machining process.

In this work, mathematical models for predicting static and dynamic cutting forces in pocket milling were developed in MATLAB® and verified experimentally. In the dynamic cutting force model, the instantaneous undeformed chip thickness was modelled to include the dynamic modulations caused by the tool vibrations so that the dynamic regeneration effect which leads to chatter is taken into account. This model was found to be more accurate in predicting cutting forces than the commonly used static models.

A chatter stability prediction criterion was proposed in which a force ratio defined

as the ratio of maximum dynamic cutting force to maximum static cutting force was employed as an indicator of chatter occurrence. This ratio has a limit value beyond which the machining process becomes unstable and is dependent on the cutter and workpiece materials. A weighting criteria was applied so as to optimize the tool path generated for chatter avoidance, minimizing forces acting on the tool and minimizing machining time.

Experiments were carried out using an 8mm HSS helical cutter and Aluminium 7075-0 workpiece and the limiting value of force ratio was 1.238. The experimental results were in good agreement with the prediction model.

The influence of roughing tool path strategy on machining time, cutting force and chatter vibration was investigated and analysed, for zigzag, parallel spiral and true spiral tool paths. The zigzag tool path was found to have the least machining time, while the true spiral tool path was found to have the least average cutting forces.

The thesis presents an investigation and analysis of end milling of pockets and the influence of roughing tool path strategy on the resultant cutting forces, chatter vibrations and machining time.

CHAPTER 1

INTRODUCTION

1.1 Background

Metal machining is the most dominant and most important operation in the manufacturing industry [1]. Among all the different metal machining processes, milling is one of the most widely used due to its flexibility in producing a wide range of products. With the competitiveness of manufacturing industries today, it is a continuing challenge to produce products of the highest possible quality, with the least amount of time and at a low cost. In the machining industry, cost-effectiveness and product quality can be achieved through optimization of the machining processes [2].

Modern CNC machines have become quite sophisticated but an efficient tool path is very crucial. The generation or selection of tool path based on the geometric definition of a work piece and the cutter without consideration of dynamic factors limits the productivity of a CNC machining system.

One of the most common operations in machining metal parts is pocket milling. This involves the manufacture of a part from a billet or forging by removing all material inside a closed boundary to a fixed depth. It is also referred to as 2.5D machining since all the machining is initially done in one plane, with a single dimension in the third axis at each point (2D). The depth in the third axis is however increased gradually, eventually achieving machining in three dimensions. These pockets may have straight edges, curved edges or a combination of both. The cutting tools used in this operation are flat-end mills with two or more flutes. Mostly, they are made of high speed steel(HSS), carbide, while some have Titanium coatings.

More than 80% of all mechanical parts which are manufactured by milling machines can be cut by Numerical Control (NC) pocket machining [3]. This is based on the fact that most mechanical parts consist of faces parallel or normal to a single plane. Also, free-form objects can be produced from a block workpiece by 2.5D roughing (pocketing) and 3D-5D finishing. The efficiency of a pocket milling tool path is therefore quite important in Computer Aided Manufacturing (CAM), and thus, improvement of tool paths can have a widespread impact in the manufacturing industry.

Most of the current Computer Aided Design and Computer Aided Manufacturing (CAD/CAM) systems, such as Computer Aided Three-dimensional Interactive Application (CATIA), Computer Augmented Design and Manufacturing (CADAM) and Mastercam®, provide the capability of generating NC machining instructions based on the geometric definition of a work piece and the cutter, thus automating part programming. However, other process parameters such as values of the spindle speed, feed rate, depth-of-cut and the cutting direction have to be decided and specified by the part programmer. Since most decisions on CNC machining parameters are made based on the intuition and experience of the operator, these processes are often carried out at conditions that are not optimal. This results in products of compromised surface quality, while using longer than necessary machining times, and hence shortening tool life.

Extensive research towards optimization of machining parameters such as spindle speed, feedrate and depth of cut has been carried out in the recent past. However, optimization of tool path has not received as much attention.

1.2 Tool paths

Tool path refers to a series of coordinate locations that a cutting tool follows in the machining process. Traditionally, tool paths are classified into two categories, roughing and finishing tool paths. A roughing tool path is used in the CAD/CAM CNC programming phase for removing most of the material, as accurately and as efficiently as possible. Some types of roughing tool paths are:

- Face milling tool paths
- Profile milling tool paths
- Pocket milling tool paths
- Engraving tool paths
- Thread milling tool paths

Finishing tool paths are then used to remove a small amount of material and to give the part the desired surface quality in the least amount of time to complete the machining process. Tool path generation softwares have been under development giving rise to more more efficient, faster and more robust tool paths, in terms of what can be achieved during machining.

A wide choice of roughing tool path strategies is provided in CAD/CAM software. For example, Mastercam® provides up to seven tool path strategies for a simple rectangular-pocket milling operation. This leaves wide room for improvement of tool path efficiency. Efficiency of tool paths has been improved by creating longer path sections which maintains cutting force near constant, rounding corner sections and ensuring few and gradual changes in cutting direction.

Tool path approaches available in CAD/CAM systems for milling of pockets can be broadly classified into two categories, contour-parallel and direction parallel

tool paths. Direction-parallel approach has two major variations, unidirectional zig and bi-directional zigzag tool paths [3].

Contour-parallel tool paths

Contour parallel tool path pattern is generated by successive offset curves along the work boundary. The algorithms to generate this pattern use a Voronoi diagram or a pixel-based approach to compute the offset curves, which are linked together to form a connected tool path. The cutter is kept in contact with the work most of the time thus less idle time spent in retracting, positioning and plunging [4]. It is widely used for large scale material removal. A contour-parallel tool path is shown in Figure 1.1.

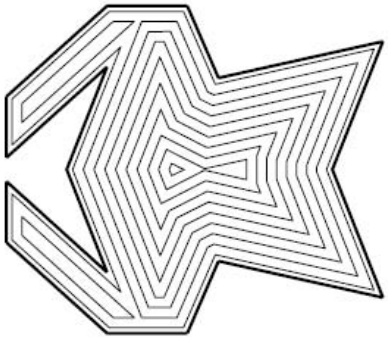

Figure 1.1. Contour-parallel tool path

Direction-parallel tool-paths: A direction-parallel tool path is illustrated in Figure 1.2.

Zig: uni-directional In these tool paths the tool is retracted at the end of each cut in one direction, and is retraced to the start of the new pass without cutting on the return stroke. Tool retraction leads to a considerable amount of idle time, during retracting the tool and returning it to the start position. It also lengthens the machining path and could negatively affect the tool life [4]. However a consistent chip removal can be maintained.

Direction-parallel tool-paths:

Zigzag: bi-directional The tool cuts both in the forward and the backward motion. The tool is not retracted at the end. As a result of minimal tool retractions, burr formation is avoided which occurs at the point of the tool leaving the workpiece while engaged.

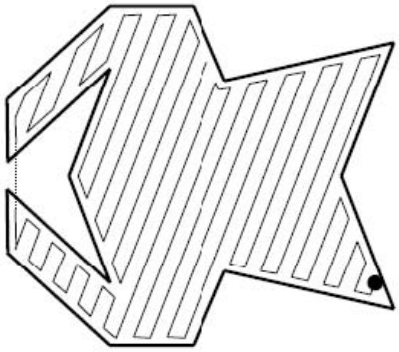

Figure 1.2. Direction-parallel tool path

Besides modification of tool paths generated by CAD/CAM softwares, improvement of tool paths can also be done through evaluation of the quality and efficiency of the alternative solutions, in terms of factors such as cutting forces, chatter vibrations and machining time. To achieve this, a geometric analysis of the cutting tool as well as dynamic characteristics of the machine/tool interaction is necessary.

Chatter, a self-excited vibration, is also a limitation of productivity with negative effects including poor surface quality, dimensional inaccuracy, and disproportionate tool wear [5]. In pocket milling, the tool paths are characterized by many changes in direction and velocity of the tool as the tool encounters corners. Cutting forces vary during tool plunging and retraction which sometimes leads to chatter. Hence the need to study and predict its occurrence.

Predicting chatter occurrence is still the subject of much research but the regeneration theory suggested by Tobias [6] is still the most comprehensive explanation for the occurrence of chatter vibration. A wavy surface left by a previous tooth during milling and removed by the successive tooth may result in the chip thickness growing, which in turn results in increasing vibrations. The forces on the tool in that case increase and may chip the tool and produce a poor finish. [3]. The dynamic cutting force acting on the cutter and workpiece also significantly determines the occurrence of self-excited chatter vibration during cutting process.

This thesis presents a model to select optimal tool path parameters for milling pockets at minimum cycle times and cutting forces, while avoiding chatter vibration.

1.3 Problem Statement

Conventional tool-path generation strategies are designed to generate tool paths that satisfy geometric requirements. They, however, do not put other physical and dynamic factors into consideration; consequently, chatter and reduced tool life are common issues in CNC machining operations, especially when machining at high speeds and when machining hard materials such as high carbon steels and carbides. Decisions on machining parameters are left to the intuition and experience of the machine operator and hence . In addition, the conventional tool paths exhibit, momentarily, rises in cutting resistance at corner sections, leading to chatter or even tool breakage.

With the continuing challenge to produce high quality products at the lowest cost, application of optimized tool paths is usually a missing link. There is a need to develop algorithms that can generate a tool path that is optimal for the

particular pocket profile that is being machined.

Most of the research in optimizing pocket milling tool path is specified to only one or two tool path strategies [7–9]. By investigating the existing tool path strategies an optimized tool path can be generated for a particular pocket profile. Chatter vibration will be minimized by providing a smooth variation in cutting resistance for sections where there is a sudden rise or decrease of cutting forces. This will result in better surface quality and it will improve tool life and machining time. This research therefore aims to optimize the pocket milling tool path with the aim of eliminating chatter and reducing machining time.

1.4 Objectives

The main objective in this project was to develop an algorithm for determination of optimal pocket milling process parameters, which minimize machining time, minimize cutting forces acting on the tool and enable chatter avoidance. To achieve this, the following specific objectives were undertaken:

1. Development of static and dynamic force models for end milling
2. Prediction of occurrence of chatter vibration for various tool path strategies
3. Development of a control algorithm to generate the optimal pocket milling process parameters
4. Experimental evaluation of effectiveness of the proposed control algorithm in machining of pockets

1.5 Significance of study

Global trends in manufacturing process are towards better quality components and lowering cost of production. No matter how advanced a CNC machining center is, the tool and the tool path can limit its productivity, especially considering that conventionally, generation of tool paths is done based on the experience of the operator. The results of this study will assist in improving the surface quality of components made by pocket milling, and also reduce the rate of tool wear by avoiding tool paths that exhibit work-tool chatter vibrations. Optimization of tool path with consideration of physical and dynamic factors will improve productivity, since tool path has been described as a weak link in machining [10]. This study will also add to the further development of tool path generation algorithms currently in use.

CHAPTER 2

LITERATURE REVIEW

2.1 Geometry of flat end mill

End mills come in a variety of material, sizes and geometries. The most commonly used are flat end mills and ball end mills. Flat end mills are often used for roughing while ball end mills are used for finishing and machining of complex surfaces. The teeth maybe straight (parallel to the axis of rotation) or at a helix angle. The helix angle helps a slow engagement of the tool, thus distributing the forces. The cutter may be right-hand (to turn clockwise) or left-hand (to turn counterclockwise). Figure 2.1 shows a typical end milling cutter.

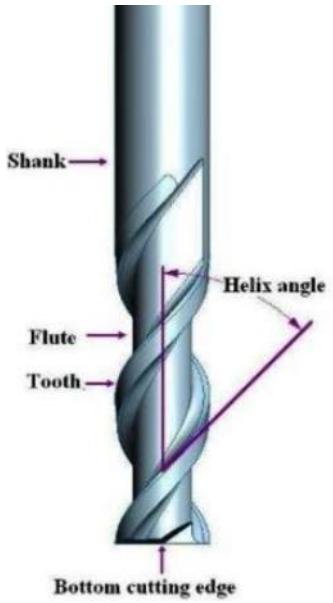

Figure 2.1. End mill cutter

2.2 Milling operations

Milling is an intermittent multi-point operation which involves feeding the work-piece into a rotating cutter. The milling operation can generally be divided into two categories: peripheral and face milling. In peripheral milling, the cut surface is parallel to the axis of the cutting tool while in face milling, the working surface is perpendicular to the axis of the cutting tool.

Helical end mills are used in peripheral milling where the walls of the part are the target finished s urface. T he h elix p roduces a g radually i ncreasing c hip load along the flutes. F igure 2.2 s hows a m odel of a h elical e nd m ill whereby.

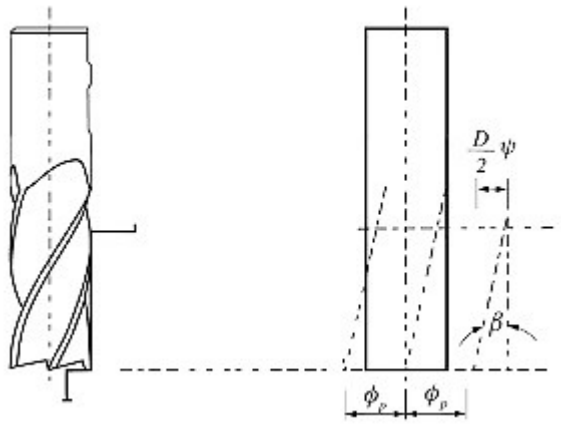

Figure 2.2. Model of helical end mill

If the helix angle on the cutter is β, a point on the axis of the cutting flute lags behind with a lag angle ψ at the depth of cut, z, which is given by

$$\tan\beta = \frac{D\psi}{2z} \tag{2.1}$$

and

$$= \frac{2z\tan\beta}{D} \tag{2.2}$$

Therefore, when the bottom end of a particular flute is at immersion angle ϕ,

a point that is axially z mm above will have an immersion angle given by $(\phi - \psi)$. The chip thickness removed is thus different at each point. End milling or peripheral milling comprises of two operations namely Up milling and Down milling, which are shown in Figure 2.3 [11].

2.2.1 Up milling

In up milling, also referred to as Conventional milling, the rotation of the cutter is against the workpiece feed direction. The entry angle is zero and the exit angle is nonzero, thus the chip is very thin at the beginning and increases in thickness along its length.

The cutter tends to push the work along and lift it upwards from the table, tending to loosen the workpiece from the fixture. In up milling, chips can be carried into the newly machined surface, causing the surface finish to be poorer than in down milling [11].

2.2.2 Down milling

In down milling, sometimes referred to as climb milling, the direction of the cutter rotation is the same as the feed direction. It is advantageous in that the work piece is pulled towards the cutter eliminating loosening of the work from the fixture or table. However, the maximum chip thickness is at the point of tooth contact with the work piece, since the entry angle is non-zero. This results in faster wearing of the cutter teeth especially if the work material is hard. This method is probably the most common option on the shop floor and will normally produce a better surface finish [11].

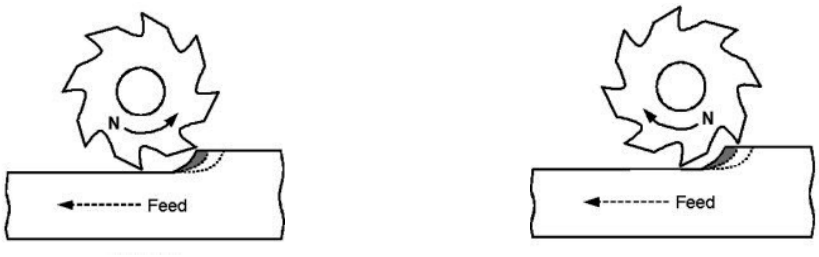

(a) **(b)**

Figure 2.3. (a) Up milling (b) Down milling

2.3 Modelling of end milling forces

Prediction of cutting forces is essential for design of machine tool structure and cutting tools as well as for the planning, control and optimization of machining processes [12]. A reliable cutting force model for the accurate prediction of cutting forces is critical to carrying out optimal machining process planning as well as well as for online adaptive control for efficient and precision machining.

Modelling of cutting forces is also one of the most important constraints in tool path optimization algorithms. These force prediction models are important as they minimize the need for experiments, thus minimizing machining cost and time.

Modelling of cutting forces requires the knowledge of the tool geometry, part geometry as well as the cutting conditions. Tool- workpiece behaviour and performance attributes such as tool wear, machine-tool chatter, dimensional accuracy, surface quality and the productivity of the system can be studied based on force analysis [13].

Several predictive cutting force models for flat-end and ball-end milling processes have been developed [13–16]. These force models generalize the relationship between instantaneous cutting forces and the chip load distribution. Therefore they can be applied in prediction of cutting forces for the geometries at hand.

In the static force model, each tooth of a helical end milling cutter is discretised into a number of elements along the cutter axis as shown in Figure 2.4.

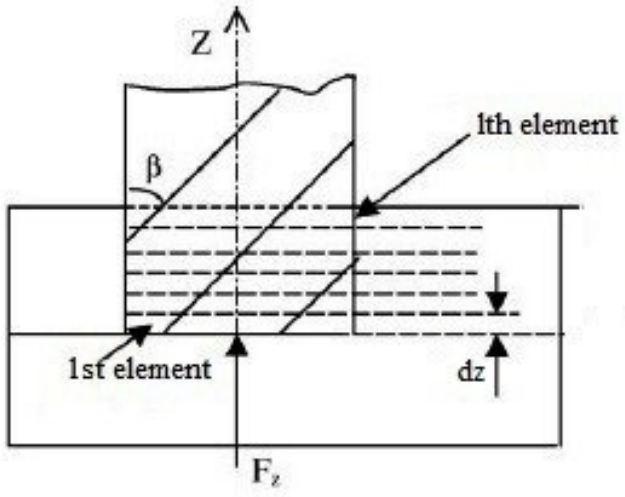

Figure 2.4. Cutter model

The principal forces acting on a differential element of height dz on the cutting edge j are Tangential($dF_{t,j}$), Radial($dF_{r,j}$) and Axial($dF_{a,j}$) forces. These are shown in Figure 2.5. Axial force is parallel to the tool axis.

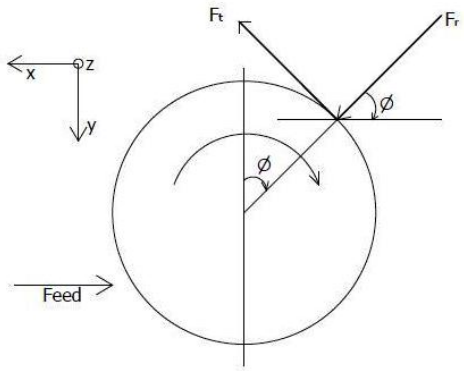

Figure 2.5. Force components on cutter

Tangential ($dF_{t,j}$), Radial ($dF_{r,j}$) and Axial ($dF_{a,j}$) forces acting on a differential element on tooth j of height dz in the axial direction are expressed as

$$
\begin{aligned}
dF_{t,j}(\phi, z) &= [K_{t,c} h_j(\phi_j(z)) + K_{te}] dz, \\
dF_{r,j}(\phi, z) &= [K_{r,c} h_j(\phi_j(z)) + K_{re}] dz, \\
dF_{a,j}(\phi, z) &= [K_{a,c} h_j(\phi_j(z)) + K_{ae}] dz,
\end{aligned} \tag{2.3}
$$

where the static chip thickness for the lth element at rotation angle ϕ is given by

$$
h_j(\phi, z) = c \sin \phi_j(z). \tag{2.4}
$$

Here, c denotes feed per tooth.

The total cutting force is calculated by adding the effort on each edge discrete cutting element. Cutting force is calculated based on the undeformed chip thickness, cutting conditions and specific cutting coefficients [16]. The coefficients K_t, K_r and K_a are cutting constants in tangential, radial and axial directions for the specific cutter-workpiece combination.

These differential elemental forces are then resolved into the feed(x), normal and axial directions using the following transformation

$$
\begin{aligned}
dF_{x,j}(\phi_j(z)) &= -dF_{t,j} \cos \phi_j(z) - dF_{r,j} \sin \phi_j(z) \\
dF_{y,j}(\phi_j(z)) &= dF_{t,j} \sin \phi_j(z) - dF_{r,j} \cos \phi_j(z) \\
dF_{z,j}(\phi_j(z)) &= dF_{a,j}
\end{aligned} \tag{2.5}
$$

To relate the cutting forces to the tool path geometry, the calculation of axial tool engagement and radial depth of cut has to be done for any position. However, in

pocket milling the axial engagement is constant for every machining pass but the radial depth of cut varies along the tool path. Depth of cut also influences the occurrence of chatter vibrations, which consequently leads to faster tool wear and poor surface quality. Predicted cutting forces are useful in avoiding tool vibration and breakage, and reducing dimensional errors caused by tool deflections.

Literature describes various studies in modelling of cutting forces, both for flat end milling and ball end milling. A study by Dang et al [14] proposed a cutting force model for flat end milling. The novel feature of their model was that the overall cutting forces caused by both the flank edge and the bottom edge cuttings were simultaneously taken into consideration. The model showed that for small axial depths of cut the bottom edge had a significant effect on total cutting forces.

A closed form expression for the dynamic forces in milling process, as functions of cutting parameters and tool/workpiece geometry was presented by Wang et al [15].

The cutting force function was characterized by the chip thickness variation and radial cutting configuration. The analysis of cutting forces was extended into the Fourier domain by taking the frequency multiplication of the transforms of the three component functions.

Kline and DeVor [17] developed a flat end milling force model based on chip load cutting geometry and the relation between cutting forces and and chip load in thin disk-shaped sections along the cutter axis. The cutter action on each cutting edge element in flat end milling is the same for all axial positions on the cutter.

Omar et al [16] introduced a generic and improved cutting force model. The model simultaneously predicted the conventional cutting forces and the surface topography during side milling operation. Effects of tool run-out, tool deflection, system dynamics, flank face wear, and tool deflection on the surface roughness

were incorporated in the model. In their work, an improved technique to calculate the instantaneous chip thickness was also presented.

2.4 Identification of Cutting Constants

2.4.1 Determination of cutting constants from orthogonal cutting

In orthogonal cutting, the cutting edge is perpendicular to the direction of tool-workpiece motion. The cutting forces are thus exerted in only two directions, the tangential and the feed direction.

Cutting coefficients are determined based on three parameters, shear angle, ϕ_s, friction angle, β_a, and shear strength, τ_s. These parameters depend both on the material and process. The shear angle, which is a function of rake angle, α_r and chip compression ratio, r_c, is determined by

$$\tan \phi_c = \frac{r_c \cos \alpha_r}{1 - r_c \sin \alpha_r}, \tag{2.6}$$

where r_c is given by

$$r_c = \frac{h}{h_c}$$

where h is undeformed chip thickness and h_c is chip thickness.

The orthogonal cutting tests are perfomed under different feedrates and cutting speeds and the resultant cutting force, F, is measured. According to [18], the tangential and feed forces can then be determined from resultant force using the relations

$$F_t = F\cos(\beta_a - \alpha_r),$$

$$F_f = F\sin(\beta_a - \alpha_r),$$

where β_a is the friction angle, α_r is the tool rake angle and ϕ_c is the shear angle.

In terms of shear stress the forces can be expressed as

$$F_t = bh\tau_s \left[\frac{\cos(\beta_a - \alpha_r)}{\sin\phi_c \cos(\phi_c + \beta_a - _r)}\right] \tag{2.7}$$

and

$$F_f = bh\tau_s \left[\frac{\sin(\beta_a - \alpha_r)}{\sin\phi_c \cos(\phi_c + \beta_a - \alpha_r)}\right]. \tag{2.8}$$

In metal machining, the parameter specific cutting pressure or tangential cutting force coefficient, K_t is defined as

$$K_t = \tau_s \frac{\cos(\beta_a - \alpha_r)}{sin\phi_c cos(\phi_c + \beta_a - \alpha_r)} \tag{2.9}$$

and the feed force constant, K_r is

$$K_r = \tau_s \frac{\sin(\beta_a - \alpha_r)}{sin\phi_c cos(\phi_c + \beta_a - \alpha_r)} \tag{2.10}$$

Attempts at theoretical evaluation of shear angle has led to two main approaches, namely the maximum shear stress principle and the minimum energy principle [18].

In the first approach, Krystof proposed a shear angle relation based on the maximum shear stress principle which states that shear occurs in the direction of the maximum shear stress. The resultant force makes an angle, $(\phi_c + \beta_a - \alpha_r)$, with the shear plane and the angle between the maximum shear stress and the principal stress must be $\pi/4$, thus leading to the shear angle relation which is expressed as

$$\phi_c = \frac{\pi}{4} - (\beta_a - \alpha_r). \tag{2.11}$$

The second approach by Merchant proposed applying the minimum energy principle. By taking the partial derivative of the cutting power given by $P_t = F_t V$ where V is cutting velocity and

$$F_t = bh \left[\tau_s \frac{\cos(\beta_a - \alpha_r)}{\sin \phi_c \cos(\phi_c + \beta_a - \alpha_r)} \right]. \tag{2.12}$$

The shear angle is obtained as

$$\phi_c = \frac{\pi}{4} - \frac{\beta_a - \alpha_r}{2}. \tag{2.13}$$

2.4.2 Orthogonal to oblique cutting transformation

In the case of helical end milling, the cutting edge is not perpendicular to the feed direction but is inclined at an angle equal to the helix angle. The tangential (K_{tc}), radial ($K_{rc)}$ and axial (K_{ac}) cutting coefficients for oblique cutting as proposed by Budal et al [19] are given by

$$
\begin{aligned}
K_{tc} &= \frac{\tau}{\sin\phi_n}\frac{\cos(\beta_n-\alpha_n)+\tan i\tan\eta\sin\beta_n}{\sqrt{\cos^2(\phi_n+\beta_n-\alpha_n)+\tan^2\eta\sin^2\beta_n}} \\
,[10pt]K_{rc} &= \frac{\tau}{\sin\phi_n\cos i}\frac{\sin(\beta_n-\alpha_n)}{\sqrt{\cos^2(\phi_n+\beta_n-\alpha_n)+\tan^2\eta\sin^2\beta_n},} \\
K_{ac} &= \frac{\tau}{\sin\phi_n}\frac{\cos(\beta_n-\alpha_n)+\tan i-\tan\eta\sin\beta_n}{\sqrt{\cos^2(\phi_n+\beta_n-\alpha_n)+\tan^2\eta\sin^2\beta_n},}
\end{aligned}
\tag{2.14}
$$

where

$$
\begin{aligned}
\tan(\phi_n+\beta_n) &= \frac{\cos\alpha_n\tan i}{\tan\eta-\sin\alpha_n\tan i} \\
\tan\beta_n &= \tan\beta_a\cos\eta \\
\tan\phi_n &= \frac{r_c(\cos\eta/\cos i)\cos\alpha_n}{1-r_c(\cos\eta/\cos i)\sin\alpha_n}
\end{aligned}
\tag{2.15}
$$

where ϕ_n is the normal shear angle in oblique cutting α_n is the normal rake angle and η is the chip flow angle. The assumptions made in determining oblique cutting coefficients from orthogonal cutting coefficients are that:

$$
\phi_n = \phi_c, \alpha_n = \alpha_r, \eta = i \tag{2.16}
$$

2.4.3 Mechanistic approach

Orthogonal cutting parameters such as shear stress, shear angle and friction coefficient have often been used to determine oblique cutting constants. However, for cutting tools with complex cutting edges the process of determining orthogonal data is tedious and time consuming. Mechanistic approach is a quick method

whereby a set of milling experiments are conducted at different feed rates but at constant immersion angle and axial depth of cut. The average forces per tooth period are then measured. The values for cutting forces obtained experimentally are equated to the those derived analytically leading to identifying the values of cutting constants. These cutting forces are independent of helix angle since material removed per tooth period is constant [19].

Since the flute cuts only within the immersion zone, that is $\phi_{st} \leq \phi \leq \phi_{ex}$, then $dz = a$, $\phi_j(z) = \phi$, and $k_\beta = 0$. Integrating the result over one revolution and dividing by the pitch angle gives the average milling forces per tooth period which is

$$\overline{F}_q = \frac{1}{\phi_p} \int_{\phi_{st}}^{\phi_{ex}} F_q(\phi) d\phi. \tag{2.17}$$

For convenience, full immersion condition where entry and exit angles are $\phi_{st} = 0$ and $\phi_{ex} = \pi$ respectively, is considered. The average cutting forces per tooth period when simplified are given in Equation 2.18.

$$\begin{aligned} \overline{F}_x &= -\frac{Na}{4} K_{rc} c - \frac{Na}{\pi} K_{re} \\ \overline{F}_y &= -\frac{Na}{4} K_{tc} c + \frac{Na}{\pi} K_{te} \\ \overline{F}_z &= +\frac{Na}{\pi} K_{ac} c + \frac{Na}{2} K_{ae} \end{aligned} \tag{2.18}$$

where N is spindle speed in revolutions per minute, a is axial depth of cut and f is feedrate.

2.5 Calculation of instantaneous depth of cut

The chip thickness can be calculated at any instant based on the current tooth position and the workpiece surface coordinates for the surface from the previous tooth pass. The interference region(flank contact area or volume) between the just cut-surface and the current position of the tool can also be determined from the relief angle and the flank length. First, the tool/workpiece contact geometry is discretised into a number of axial slices, n layers. The instantaneous chip thickness is calculated using a circular interpolation method between two points left by the previous tooth, n_{t-1} on the previous arc surface, and the current tool tip position on the current arc surface

For each time step the instantaneous tooth position at the current axial layer is identified. The formation of the chip is illustrated in Figure 2.6.

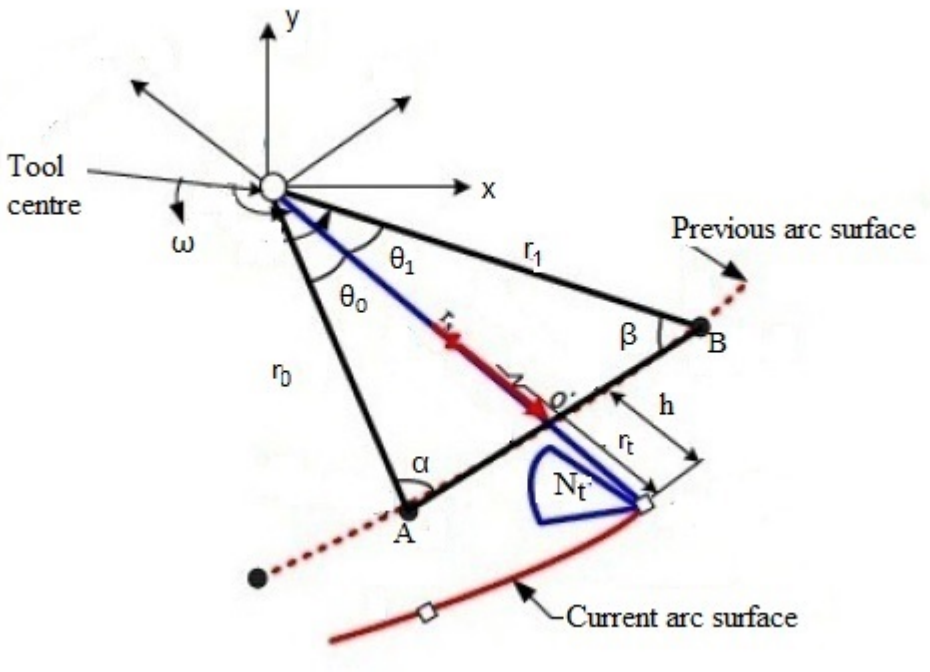

Figure 2.6. Geometry of chip

2.6 Model system dynamics

The system displacements that are caused by the cutting forces are obtained by modelling the structural dynamics of the flexible tool-workpiece setup. The model used for machining dynamics is shown in Figure 2.7

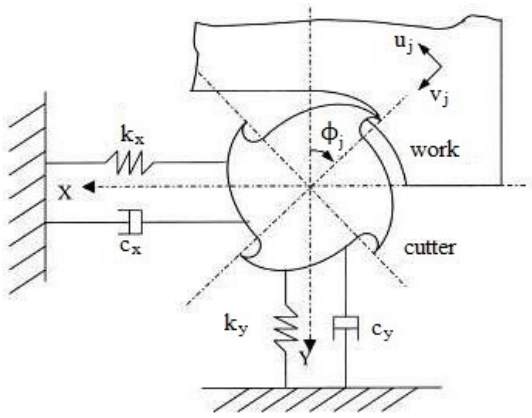

Figure 2.7. Chip formation in milling

The cutter is considered to be a one-degree-of-freedom spring-damper vibratory system in the two orthogonal directions x and y. The cutting forces exciting the system in the feed (x) and normal (y) directions cause dynamic displacements x and y, respectively. These displacements are then fed back to the milling kinematics model. The dynamics of this milling system can be represented by the differential equations of motion as [18]

$$\begin{aligned} m_x\ddot{x} + c_x\dot{x} + k_x x &= F_x(t), \\ m_y\ddot{y} + c_y\dot{y} + k_y y &= F_y(t), \end{aligned} \tag{2.19}$$

where m_x and m_y are the masses, c_x and c_y are the damping coefficients, and k_x and k_y are the stiffness of the machine tool structure in directions x and y,

respectively, while F_x and F_y are the components of the cutting force that are applied on the tool in the directions of x and y and respectively.

The differential equations are solved using the 4th order Runge-Kutta method since it is accurate [20]. The continuous variable t is replaced by the discrete variable t_i, and using a constant time increment δt the equations are solved from initial conditions.

The equations of motion are solved in the time domain using a Simulink model to calculate the vibrations in the system, which are consequently used in the calculation of instantaneous dynamic chip thickness.

2.6.1 Dynamic regenerative undeformed chip thickness

In the dynamic milling process, the tooth leaves behind a wavy surface as explained earlier, thus the undeformed chip thickness will not only be affected by the instantaneous vibration but also by the amount of waviness left by the previous tooth. The resulting thickness thus comprises of two parts, the static, h, and dynamic components caused by the present tooth period (inner modulation), v_j and previous tooth period (outer modulation), ${v_j}^o$. The instantaneous dynamic regenerative undeformed chip thickness for the j-th tooth at an angular position ϕ_j can be expressed as

$$(h - v_j + {v_j}^0)g(\phi_j), \tag{2.20}$$

where h is the instantaneous undeformed chip thickness in steady state cutting condition which can be determined from the feed per tooth, f_t as

$$h = f_t \sin \phi_j. \tag{2.21}$$

where $g(\phi_j)$ is a unit step function that determines whether the tooth is in cut or out of cut, which means that

$$\begin{aligned} g(\phi_j) = & \quad 1, for \phi_{st} < \phi_j < \phi_{ex} \\ g(\phi_j) = & \quad 0, for \phi_j < \phi_{st} or \phi_j > \phi_{ex}, \end{aligned} \tag{2.22}$$

where ϕ_{st} and ϕ_{ex} are the start and exit immersion angles of the cutter.

For instantaneous deflections in the x and y($y - y_0$) directions, x and y, the inner modulation v_j is given by

$$v_j = x \sin \phi_j + y \cos \phi_j. \tag{2.23}$$

The dynamic milling process is nonlinear in that the outer modulation is not necessarily left by the previous tooth, $j+1$, but could be left by the $j+2$, $j+3$, $j+4$ tooth especially at high amplitudes of modulation. Thus the Equation 2.24 is an approximation for outer modulation [18].

$$v_j = \min \{v_{j+1}(t-T), v_{j+2}(t-2T) + h, v_{j+3}(t-3T) + 2h, ...\} \tag{2.24}$$

where t is the current time and T is the time period between successive tooth engagements and is given by

$$T = \frac{2\pi}{N n_t}, \tag{2.25}$$

where N is the spindle speed and n_t the number of flutes/teeth.

It is assumed that the dynamic cutting forces in milling change instantaneously with the changes in the undeformed chip geometry that occur due to the dynamic-regenerative effects.

2.7 Vibrations in milling

In milling the action of each tooth is intermittent and cuts less than half of the cutter revolution. This results in varying but periodic chip thickness, which together with the impact when the edge touches the workpiece causes mechanical fatigue of the material and vibrations. Vibrations in milling hinder productivity, and excess vibrations accelerate tool wear, tool chipping and result in poor surface finish [18].

These vibrations are of two kinds, namely forced vibrations and chatter vibrations. Forced vibrations are caused by periodic cutting forces acting within the machine structure. Chatter vibrations on the other hand may be explained by the wave regeneration theory, first explained by [6]. Regenerative chatter is a self-excitation vibration associated with the phase shift between successive vibration waves left on the chip.

2.8 Fundamentals of free and forced vibrations

Milling vibration can be modelled as a spring, mass and damper system of various degrees of freedom. To explain the behaviour of such a system, consider a single degree of freedom system illustrated in Figure 2.8, where m, k and c are the mass, spring and damping elements.

When there there is an external force $F(t)$, the motion of the mass is described

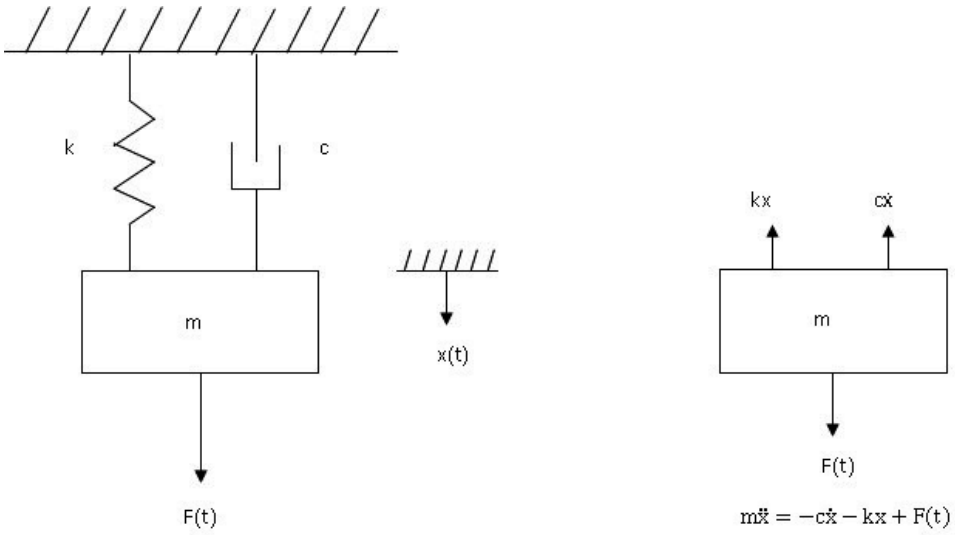

Figure 2.8. Mass, spring and damping model of a single degree of freedom system

by Equation 2.26 [18].

$$m\ddot{x} + c\dot{x} + kx = F(t) \tag{2.26}$$

When a force is applied for a short duration, or the system deviates from equilibrium, it experiences free vibrations, the amplitude of which decay with time as a function of the system's damping constant. This free vibration is illustrated in Figure 2.9.

The frequency of the vibrations depends mainly on the mass and the stiffness constant. The damping ratio, ζ is defined as $\zeta = c/2\sqrt{km}$, and is always less than one in mechanical structures, and usually less than 0.05 in most metal structures [18].

When there is an external force $F(t)$, the system experiences forced vibrations. If the force is constant $F(t) = F_0$, the system experiences free or transient vibration for a short period of time then stabilizes at a static deflection given by F_0/k. If

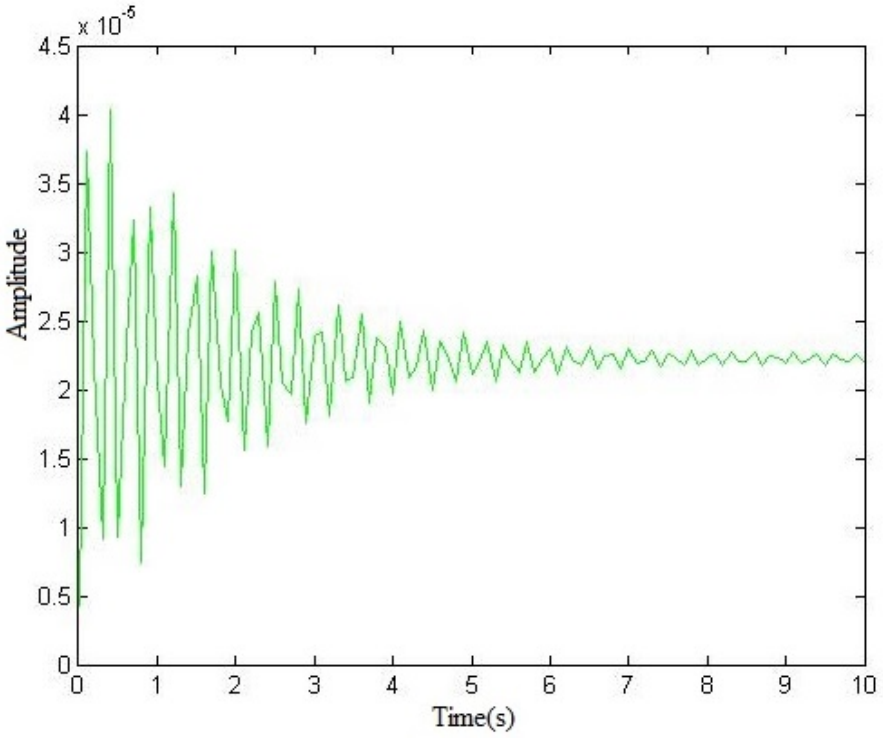

Figure 2.9. Free vibration

the forcing function is harmonic, the system equation becomes

$$m\ddot{x} + c\dot{x} + kx = F_0 \sin(\omega t) \tag{2.27}$$

The system experiences forced vibration at the same frequency, ω, as the force, but with a time delay.

2.9 Chatter Stability Criterion

Modelling of the dynamic milling process and the determination of chatter-free cutting conditions is becoming increasingly important in optimizing machining operations. Free vibrations occur when the mechanical system is displaced from its equilibrium and is allowed to vibrate freely. Forced vibrations appear due to

external excitations.

The principal source of forced vibrations in milling processes is when each cutting tooth enters and exits the workpiece. Free and forced vibrations can be avoided or reduced when the cause of the vibration is identified. However, self-excited vibrations (or regenerative chatter) extract energy from the interaction between the cutting tool and the workpiece during the machining process. This phenomenon is a result of an unstable interaction between the machining forces and the structural deflections. The forces generated when the cutting tool and part come into contact produce significant structural deflections. These structural deflections modulate the chip thickness that, in turn, changes the machining forces. For certain cutting conditions, this closed-loop, self-excited system becomes unstable and regenerative chatter occurs [21]. Regenerative chatter may result in excessive machining forces and tool wear, tool failure and poor surface finish, thus severely decreasing operation productivity and part quality [5].

2.9.1 Time Domain Simulation

Time domain analysis of systems involves the record of what happens to a parameter in the system versus time. In milling system analysis, a time domain model is used to predict cutting forces, torques, power, dimensional surface finish and the amplitudes and frequency of vibration, if any. It is used extensively since it provides realistic information regarding chatter stability and severity of chatter vibrations. It is also advantageous over other methods since it provides more insight into the dynamics of the milling operation. Tlusty and Ismail [22] described the dynamic behaviour of the milling process using this method and investigated the boundary zone between stable and unstable conditions. Tlusty and Macneil.P. [23] also used this method to carry out a comparison between sta-

bility limits obtained by an improved formulation of the dynamic cutting forces and showed significant differences from earlier models.

Ko and Altintas [24] developed a time domain model for plunge milling. In the model, two lateral vibrations, an axial vibration and a torsional vibration were considered and the fourth order Runge kutta method was used to solve the differential equations. In this way they were able to predict vibrations under the cutting forces and torques applied during plunge milling. However, time domain simulation still lacks a clear chatter stability criterion. Various methods have been used as chatter stability criteria in time domain simulation.

2.9.2 Frequency Domain Simulation

Every real wave can be broken down into a number of sine waves of different amplitudes and frequencies. These component waves form the spectrum of the signal. Frequency domain analysis involves viewing a signal from a system along the frequency axis rather than the time axis, as shown in Figure 2.10.

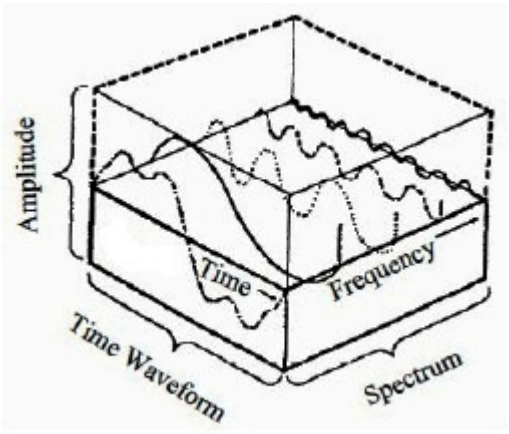

Figure 2.10. Illustration of time and frequency domains

Many engineering processes have measurements where large signals mask others in the time domain. The frequency domain provides a useful tool for analyzing

these small, but important, components.

Signals can be transformed from the time domain to the frequency domain through Fourier Transform, also called Fourier Analysis. The reverse is also possible, and is referred to as Inverse Fourier Transform (IFT). Information is neither gained nor lost when this transformation is done, but is simply a different perspective [25].

Jeon and Kah [26] developed a chatter prediction algorithm for pocket milling operation. Presence of chatter was identified by chatter marks on milled surface and frequency domain analysis of measured vibration signal. Stability limits for multi-axis milling, which is applied in milling complex geometries and surfaces, can be identified in frequency domain [27].

2.9.3 Stability lobes theory

A stability lobes diagram (SLD) shows the boundary between chatter-free machining operations and unstable processes, in terms of axial depth of cut as a function of spindle speed. Stability lobes diagrams are used to select chatter-free combinations of machining parameters. [28]. Figure 2.11 shows a simple example of a stability lobe

It is formed by a series of intersected scallop-shaped borderlines of stability. Stability diagrams can be applied in machining processes to optimize the maximum depth of cut at the highest available spindle speed, thus improving the material removal rate and increasing productivity.

Usually, for each lobe, it is stable below the lobe, and unstable above the lobe. Since the lobes intersect, points located below one lobe and above the neighboring lobe are treated as unstable.

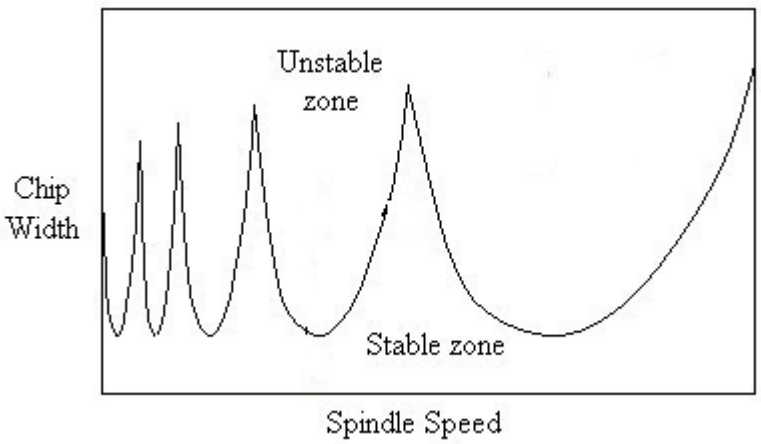

Figure 2.11. Stability Lobe Diagram
[28]

2.10 Tool path optimization

Optimization refers to a process of determining the best solution from among possible solutions. In manufacturing, optimization can be carried out with various technological goals such as:

- Achieving best possible surface quality
- Minimizing tool wear
- Achieving shortest machining time
- Minimizing machining costs

Optimizing cutting tool paths is one of the ways to achieve the global trend of improving throughput and lowering cost of production in manufacturing industry. Modern CAM softwares such as Mastercam® provide up to eight tool path strategies that can be used to machine a simple rectangular pocket, as shown in Figure 2.12.

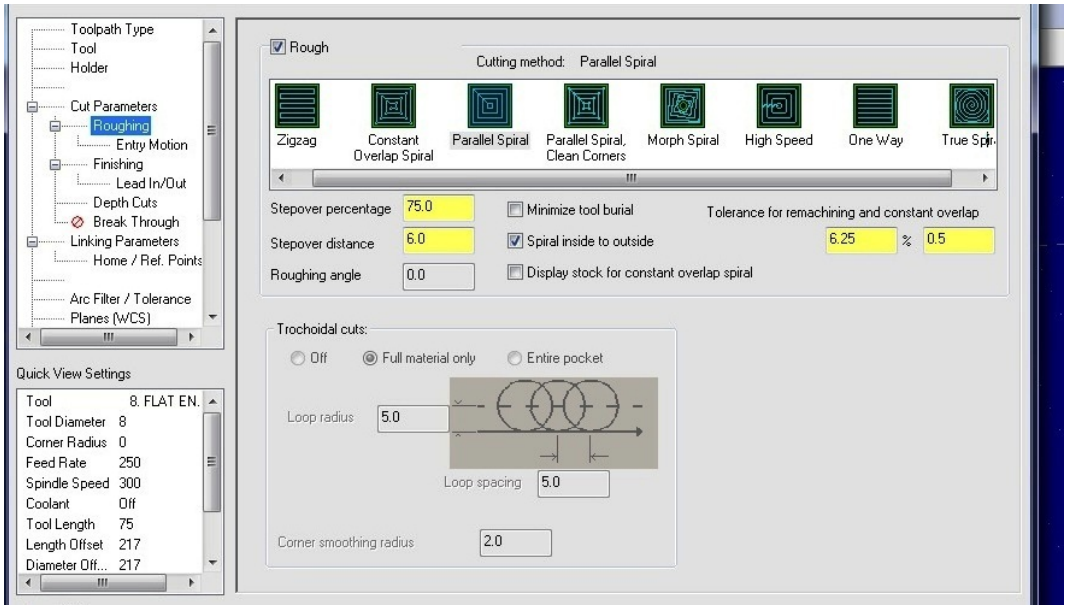

Figure 2.12. Screenshot of tool path strategies available for machining a rectangular pocket using Mastercam®

These variety of tool path strategies leaves a wide room for improvement of tool path efficiency. There exists a gap in the criteria that is used in selecting or generating the tool path to be applied in machining a pocket. By evaluating the quality and efficiency of the alternative solutions an optimal solution can be selected. In optimization of milling tool path, factors such as cutting-tool geometry and material, work piece material and geometry, machining operation and use of coolants must be taken into account. Some of the approaches that have been applied in optimizing tool paths include reduction of machining time, minimization of cutting forces, modification of corner sections and avoiding redundant tool movements and potential collisions.

Daneshmand et al [29] investigated the numerous tool paths available in two common CAD/CAM softwares, CATIA® and Mastercam® so as to determine the most suitable tool path. This was done for the roughening operation of machining a gearbox model and a disc screen, using both end mill and ball-nosed tools. They simulated the tool-path planning strategies according to the machining

time provided by the software. The accuracy of the operations verified the most suitable tools path. Their research results indicated that for Mastercam®, the minimum machining time was achieved with zig-zag strategy when using end mill, and spiral strategy when using ball-end tool. For CATIA®, the back and forth strategy gave the minimum machining time when using end mill and the inward helical strategy when using ball-nose tool. They also found that machining time changes when the geometry of the object being machined was altered.

Another approach that has been applied in selection of milling paths for complex surfaces is minimizing of dimensional errors due to tool deflection, which was presented by Lopez de Lacalle et al [30]. This resulted in an improvement on the accuracy of milled surfaces. It was based on the calculation of the minimum cutting force component, which was related to the tool deflection. In their first suggestion, a general tool path direction was selected that minimized the mean value of the tool deflection force on the surface. Based on this the CAM operator could then produce a CNC program which lead to an accuracy improvement. The second option was to create a grid of control points and select different milling directions at each control point. Joining these points, the minimum force lines were defined on the workpiece surface and used as the master guides for the tool path programming of a complete surface. After applying these methods to 3-axis milling the dimensional errors reduced from 30 mm to below 4 mm.

Choi and Cheung [31] proposed a method focused on avoiding redundant tool movements and collisions in Multi-Material Layered Manufacturing (MMLM) of heterogeneous prototypes. The approach facilitated control of MMLM and increased the fabrication efficiency of complex objects by generating multi-tool paths that avoid redundant tool movements and potential collisions. They used a topological hierarchy-sorting algorithm to group complex multi-material contours into groups connected by a parent-and-child relationship. The multi-tool

paths generated enabled sequential deposition of materials without redundant tool movements. The build time was further reduced by another tool path planning algorithm that generated collision-free multi-tool paths to control the tools that deposit materials concurrently.

Neural networks have also been applied in optimizing tool paths, as described by Korosec and Kopac [32]. They demonstrated how with the help of artificial neural network, the prediction of milling tool path strategies could be performed in order to determine which tool path strategies or their sequence would yield the best results, since any machining task may be carried out using different tool-path strategies or sequences of various strategies. The result was that only one of all possible applied strategies was optimal in terms of the desired technological goal or aim. The study was based on production of car lights equipment by the tool shop industry. Their technological aim was to achieve the best possible surface quality of machined workpieces, which they verified by measuring surface roughness.

Conventional tool paths can be modified and even additional tool paths appended to the tool paths to achieve the optimal tool path. Hyun-Chul Kim [33] presented an optimized tool path, which maintained Material Removal Rate (MRR) as constant as possible so as to achieve constant cutting forces and to avoid chatter vibrations. In his work additional tool path segments were appended to the basic tool path obtained by geometric shape using a pixel-based simulation technique. The algorithm was implemented for two-dimensional end milling operations, and cutting tests were carried out by measuring spindle current, to reflect the state of machining.

El-Midany et al [34] developed a feed rate-machining time model that took into account machine acceleration and deceleration for automatically identifying the most productive tool path pattern. The model was then used to compare the

total machining time for five common types of tool path patterns, namely, normal zigzag, smooth zigzag, normal spiral, smooth spiral and fishtail spiral. The results showed that the optimal tool path pattern was dependent on part geometry, physical characteristic of cutting tool and cutting conditions.

Pateloup et al [35], proposed a pocketing tool path improvement method that involved modification of the values of the corner radii in order to increase real feed rate. This method checked the radial depth of cut variations along the tool path. The computed tool path presented a smaller length and the machine tool produced a higher average feed rate at the same time. Use of B-splines for tool path computation was a notable improvement in this method, as compared to the use of straight lines and arcs.

Choy et al [7] suggested a corner-looping-based tool path for pocket milling. The basic pattern for the improved tool path was a conventional contour-parallel tool path. In their research they appended bow-like additional segments to the corner sections in the tool path such that corner material was removed progressively in several passes, to prevent rise in cutting resistance. The proposed tool path was implemented as an add-on user function in a CAD/CAM system.

Wang et. al. [36] proposed an integrated optimization of cutting parameters and the generation of tool path in raster milling. In their work, they proposed a methodology that optimized the cutting feed rate, the path interval, and the entry distance in the feed direction simultaneously, in order to achieve the best surface quality in a given machining time. This was achieved by implementing prediction models for surface roughness and machining time in ultra precision raster milling. The work improved surface quality without compromising efficiency of the milling process.

Tool path optimization has also been done with a goal of improving energy efficiency of CNC machines. Li et. al. [37]. In this work, the authors developed an energy consumption model. The model took into account the energy consumption, which was the performance criteria, in optimization the tool path connection. The simulated annealing and exhaustive algorithm were applied in the optimization process. The model was was proven to be achieve an energy efficient machining process.

In summary, models have been made to optimize specific tool paths such as zigzag and contour parallel tool paths. Variations of the these tool paths have also been developed such as the curvilinear tool paths currently applied in manufacture of aerospace parts, which are neither straight nor curved. However, the CNC machine operator still faces the challenge of generating the optimal tool path from all the variations available in the CAM software. Production is still being done using tool paths of which the operator has no way of knowing if they are optimal. Models that have been developed so far consider only a single factor such as speed, feedrate or depth of cut that would affect productivity, but neglect dynamic factors such as cutting force and chatter vibration.

This work is therefore meant to create a way to predict dynamic factors, that is machining time, cutting forces and chatter vibration at the point of selecting machining parameters. Pocket milling involves selecting of parameters that include the tool path strategy whose impact is investigated in this study. The selection of other parameters, that is, spindle speed, feedrate and depth of cut can then be done with a predicted view of the cutting forces and chatter vibration.

CHAPTER 3

METHODOLOGY

3.1 Identification of cutting constants

The mechanistic approach of determining milling coefficients was applied to identify cutting constants. Experimental work was done on a vertical machining center using high speed steel cutters. The workpiece material was Aluminium 7075-0. For this preliminary experiments, one-tooth cutter was used to eliminate errors due to uneven diameters at the different tool tips.

In this method, a set of milling experiments were conducted at different feed rates but constant immersion angle and axial depth of cut. The average forces per tooth period were then obtained from the measured data. The values for cutting forces obtained experimentally were equated to the those derived analytically thus the values of the various cutting constants were identified. These cutting forces are independent of helix angle since material removed per tooth period is constant.

The setup shown in Figure 3.1 was used to measure instantaneous cutting forces.

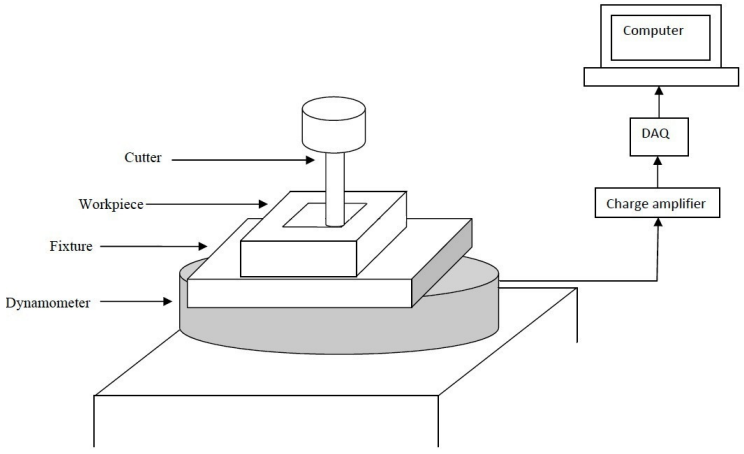

Figure 3.1. Experimental setup for determination of baseline data.

3.2 Modelling of cutting force

In the static force model, each tooth of a helical end milling cutter is discretised into a number of elements along the cutter axis. In milling process, the principal forces acting on the cutting edge are Tangential ($F_{t,j}$), Radial ($F_{r,j}$) and Axial ($F_{a,j}$) forces. These are shown in Fig. 3.2. Axial force is parallel to the tool axis.

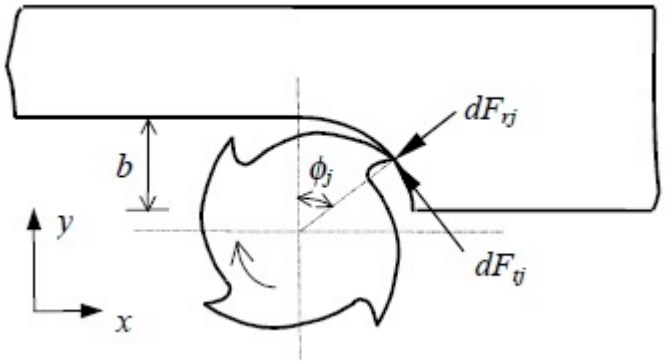

Figure 3.2. Cutter modelling

Forces acting on a differential element of height dz in the axial direction, that is, $dF_{t,j}$, $dF_{r,j}$ and $dF_{a,j}$, as explained in section 2.3, are expressed as

$$\begin{aligned} dF_{t,j}(\phi, z) &= [K_{t,f} h_j(\phi_j(z)) + K_{te}]dz, \\ dF_{r,j}(\phi, z) &= [K_{r,f} h_j(\phi_j(z)) + K_{re}]dz, \\ dF_{a,j}(\phi, z) &= [K_{a,f} h_j(\phi_j(z)) + K_{ae}]dz, \end{aligned} \tag{3.1}$$

where dz is the height of the differential element and h_j is the static chip thickness for the jth element at rotation angle ϕ. This chip thickness for a rigid system is given by

$$h_j(\phi, z) = [f_t \sin \phi_j(z)] g(\phi_j), \tag{3.2}$$

where f_t is feed per tooth.

The total cutting force is calculated by summing up the elemental forces for the entire part that is engaged with the workpiece. Cutting force is calculated based on the undeformed chip thickness, cutting conditions and specific cutting coefficients [16]. K_t, K_r and K_a are model coefficients in tangential, radial and axial directions for the specific cutter-workpiece combination. The cutting forces on tooth j in the x and y directions are obtained as

$$\begin{aligned} F_{xj} &= -F_{tj}\cos(\phi_j) - F_{rj}\sin(\phi_j) \\ F_{yj} &= -F_{tj}\sin(\phi_j) - F_{rj}\cos(\phi_j) \end{aligned} \tag{3.3}$$

where $F_{tj} = K_t a h(\phi_j)$ and $F_{rj} = K_r F_t j$.

Integration is then done along the whole axial depth to obtain the values of differential forces, which are summed to obtain the cutting force values as in Equation 3.4.

$$\begin{aligned} F_x &= \sum_{j=0}^{N-1} F_{xj}(\phi_j) \\ F_y &= \sum_{j=0}^{N-1} F_{yj}(\phi_j) \end{aligned} \tag{3.4}$$

where ϕ_j is the rotational position of tooth j and $\phi_j = \phi + j\phi_p$ and $\phi_p = \frac{2\pi}{N}$. ϕ varies with time and $\phi = \Omega t$ where Ω is the spindle angular speed in rad/s.

The model was simulated in MATLAB and is summarized in the flowchart shown in Figure 3.3. The standard model inputs were as listed in Table 3.1.

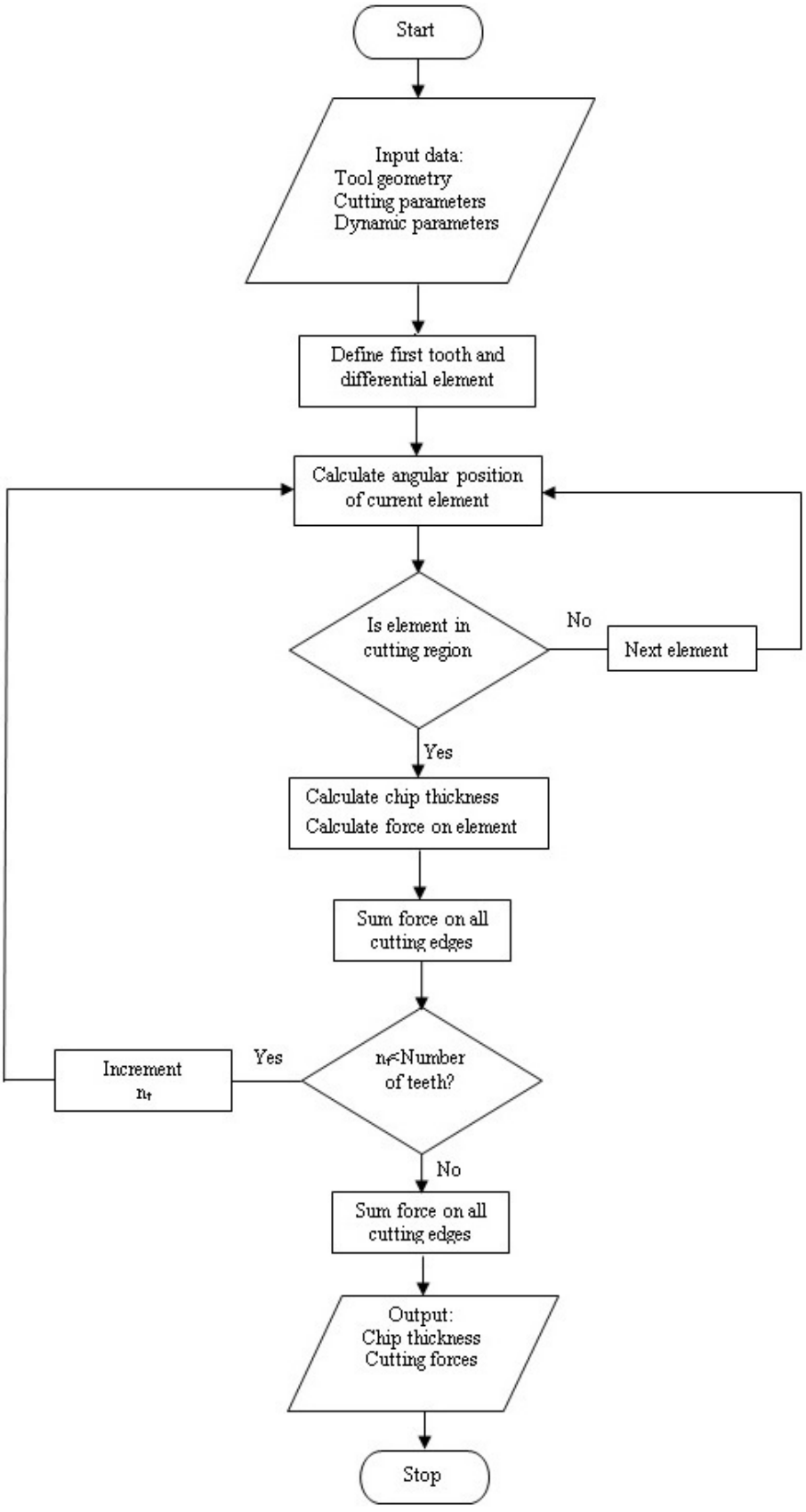

Figure 3.3. Flowchart of milling force simulation

Table 3.1: Model inputs

Input parameter	Value
Milling operation	Up milling
Axial depth(a)	2 mm
Nominal depth of cut(b)	2.4 mm
Feedrate(f)	0.2 mm/tooth
Spindle speed(N)	325 rpm
Helix angle (β)	30
Number of teeth(n_t)	2
Cutter diameter(D)	8 mm

The cutter pitch angle ϕ_p for a cutter with n_t teeth is given by Equation 3.5.

$$\phi_p = (2\pi)/n_t \tag{3.5}$$

3.2.1 Cutter engagement boundaries

Of importance in the determination of cutting forces is the cutting phase which means the cutter is engaged on the workpiece. Cutting forces occur only when the cutter is within this engagement boundary, that is $F_x(\phi) = 0, F_y(\phi) = 0, F_z(\phi) = 0$ when $\phi_{st} \leq \phi \leq \phi_{ex}$. The start and exit angle are illustrated in Figure 3.4.

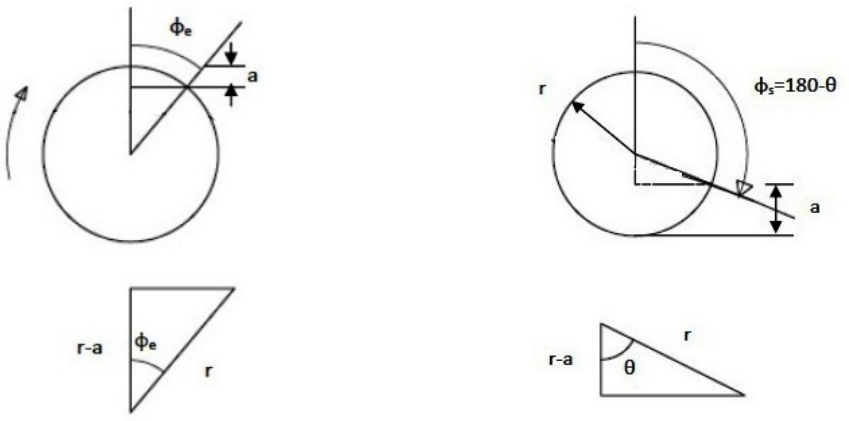

a. Up milling **b. Downmilling**

Figure 3.4: Start and exit angles

The start or entry angle in up milling is $\phi_s = 0$ while the exit angle depends on the radius of the tool,r and the nominal depth of cut, b, and is given by

$$\phi_e = \cos^{-1}(\frac{r-b}{r}). \tag{3.6}$$

In down milling, the exit angle is $\phi_e = 180°$. The start angle is dependent on the nominal depth of cut and the radius of the tool, and is given by

$$\phi_s = 180 - \theta = 180 - \cos^{-1}(\frac{r-b}{r}). \tag{3.7}$$

The start and exit angle during a milling operation can be easily visualised in the cutting force waveform, such as the one in Figure 3.5. The waveform is a predicted waveform generated from the algorithm summarized in Figure 3.3.

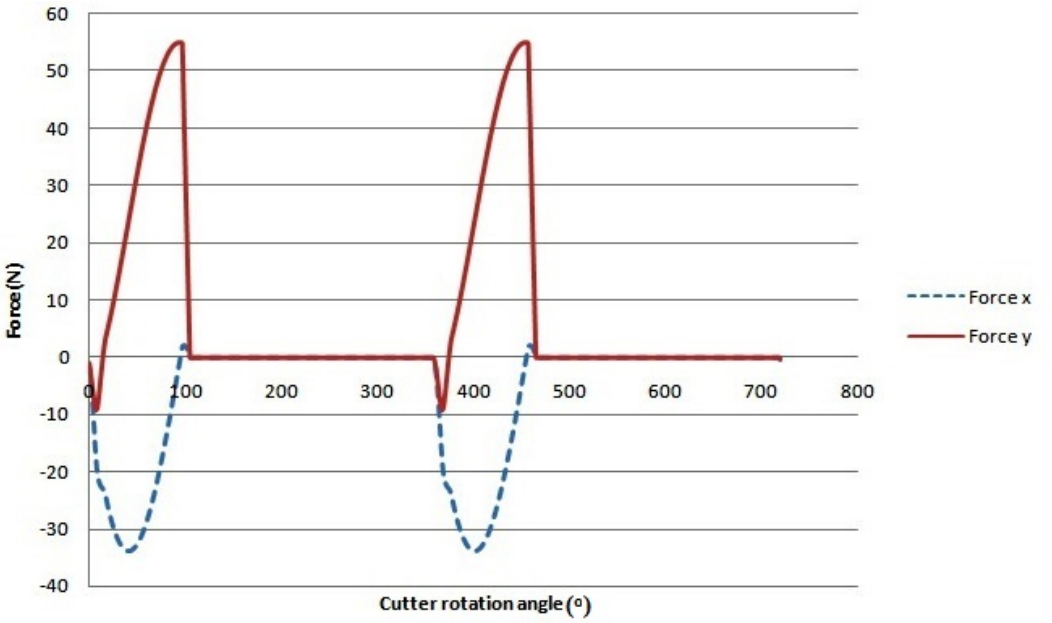

Figure 3.5. Variation of cutting force with cutter rotation angle

3.3 Dynamic milling system model

In the dynamic force model, a predictive time domain model is presented for the simulation and analysis of the dynamic cutting process and chatter in milling. The instantaneous undeformed chip thickness is modelled to include the dynamic modulations caused by the tool vibrations so that the dynamic regeneration effect is taken into account as described by Altintas [38].

The governing equations for the dynamic milling system are given in Equation 3.8.

$$\begin{aligned} m_x\ddot{x} + c_x\dot{x} + k_x x &= \sum_{j=0}^{N-1} F_{xj}(\phi_j) = F_x(t), \\ m_y\ddot{y} + c_y\dot{y} + k_y y &= \sum_{j=0}^{N-1} F_{yj}(\phi_j) = F_y(t), \end{aligned} \tag{3.8}$$

where m is the mass, c is the damping constant, and k is the spring constant. This model was implemented in MATLAB®. The dynamic milling system cannot be expressed as simple analytical functions and the dynamic differential equations which represent the system cannot be solved analytically since the system is non-linear. Numerical methods are thus used to solve these differential equations. The solution is an approximate solution, in which the continuous time variable t is replaced by a discrete time variable, and the differential equations are solved in steps, with an increment of dt. The solution starts at known initial conditions.

The model for the dynamic regenerative chip thickness is illustrated in Figure 3.6

The static undeformed chip thickness is determined from the feed per tooth as

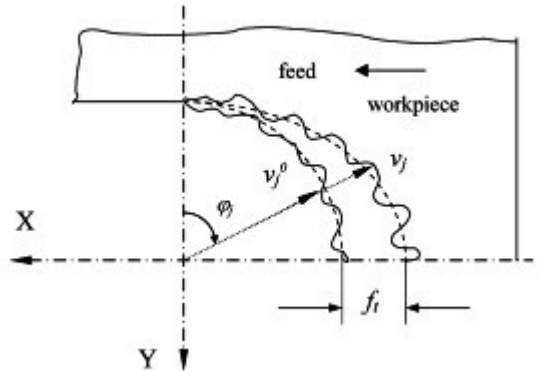

Figure 3.6. Model for dynamic regenerative chip thickness

$$h = g(\phi_j)[f \sin \phi_j], \tag{3.9}$$

where $g(\phi_j)$ is a unit step function that determines whether the tooth is in cut or out of cut.

In the dynamic milling process the undeformed chip thickness is comprised of two parts, a static part, h, and a dynamic component caused by the present tooth period (inner modulation) v_j, and previous tooth period (outer modulation) $v_j o$. The static part does not contribute to the dynamic chip load, hence the dynamic undeformed chip thickness for tooth j at an angular position ϕ_j is calculated as

$$h_d(\phi_j) = [\Delta x \sin(\phi_j) + \Delta y \cos(\phi_j)]g(\phi_j), \tag{3.10}$$

where $\Delta x = x - x_0$, $\Delta y = y - y_0$ and (x, y) and (x_0, y_0) are the dynamic displacements at the present and previous tooth periods respectively. The rotation angle varies with time, $\phi(t) = \Omega t$ where Ω is the spindle angular speed in rad/s. The tooth passing frequency $\omega = n_t \Omega$ and the tooth period $T = \frac{2\pi}{\omega}$, where n_t is the number of teeth on the cutter.

The dynamic cutting forces on tooth j in the x and y directions are obtained as

$$F_{xj} = -F_{tj}\cos(\phi_j) - F_{rj}\sin(\phi_j)$$
$$F_{yj} = -F_{tj}\sin(\phi_j) - F_{rj}\cos(\phi_j) \tag{3.11}$$

where $F_{tj} = K_t a h(\phi_j)$ and $F_{rj} = K_r F_t j$, where a is axial depth of cut.

The total dynamic milling forces for all teeth are given by

$$F_x = \sum_{j=0}^{M-1} F_{xj}(\phi_j),$$
$$F_y = \sum_{j=0}^{M-1} F_{yj}(\phi_j), \tag{3.12}$$

where ϕ_j is the rotational position of tooth j and is given by $\phi_j = \phi + j\phi_p$ and $\phi_p = \frac{2\pi}{n_t}$. ϕ varies with time and is given by $\phi = \Omega t$ where Ω is the spindle angular speed in rad/s.

The MATLAB®model is designed based on three main blocks namely; milling forces, milling kinematics, and system dynamics. The milling kinematics involve the calculation of the chip thickness. The concept of discretizing the tool/workpiece model is employed in chip thickness and cutting force computation.

The model inputs include:

1. Tool geometry parameters: number of teeth, tool diameter, helix angle, flank length

2. Cutting parameters: spindle speed, feed per tooth, depth of cut, cutting

coefficients

3. Dynamic parameters: natural frequency, mass, stiffness and damping coefficient for each mode of vibration

4. Simulation parameters: number of cycles, iterations per cycle and number of axial layers

This work proposes that the ratio of the predicted maximum dynamic cutting force, max (F_d), to the predicted maximum static cutting force, max (F_s), be used as a criterion for the chatter stability, as given in Equation 3.13. These maximum values are selected from a period of several tool revolutions. From these values, a force ratio, ρ is defined as

$$\rho = \frac{\max(F_d)}{\max(F_s)}, \tag{3.13}$$

where F_d is the cutting force predicted using dynamic cutting force model which takes into account the regenerative effect on the undeformed chip thickness, and F_s is the cutting force predicted using the static cutting force model. This ratio is used to determine whether there is chatter or not.

The model outputs are the instantaneous static and dynamic cutting forces in x and y directions, the maximum static and dynamic cutting forces and the chatter value.

3.4 Experimental work

In this section experimental procedure to verify theoretical models developed in sections 3.2 and 3.3 is outlined.

3.4.1 Tool path generation and simulation

MasterCAM CAD/CAM software was used in design of parts and generation of tool paths for the various pockets. It was also used to simulate and obtain the machining times for the various operations. To obtain the machining times when using the zigzag (direction-parallel), parallel spiral (contour parallel) and smooth spiral tool paths shown in Figure 3.10, simulation was done for the machining of a rectangular pocket measuring 30 mm by 20 mm to a depth of 10 mm.

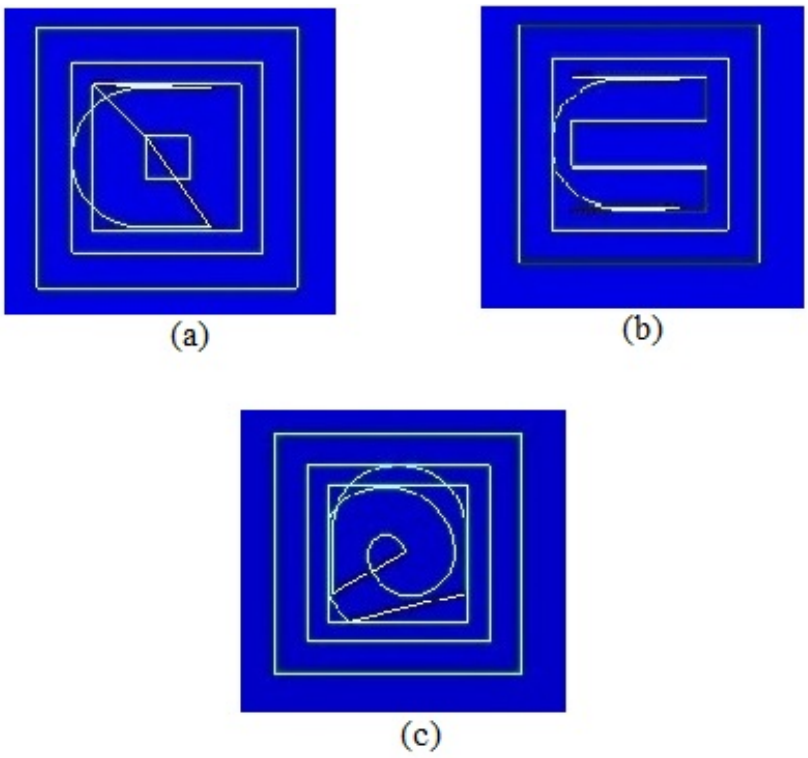

Figure 3.7. (a) Parallel spiral tool path (b) Zigzag tool path (c) True spiral tool path

Zigzag tool path: It is a direction-parallel tool path where the tool cuts both in the forward and backward direction. It results in less tool retractions than the one way tool path but also presents sharp corner cutting.

Parallel spiral: The tool cuts in a spiral motion following the pocket contour. The tool has one start and one finish position for every depth cut. It is charac-

terized by sharp corners which may necessitate the use of a smaller diameter tool for finishing the corners.

True spiral: This tool path is generally similar to the parallel spiral tool path, however the path does not follow the pocket contour but follows a true spiral path. Sharp direction changes are only encountered at the start or end of the depth cut depending on whether an inward or outward spiral was applied.

The difference in the machining times is illustrated in Figure 3.8. The machining times are stored in MS Excel document for ease of reading into MATLAB® by optimization algorithm.

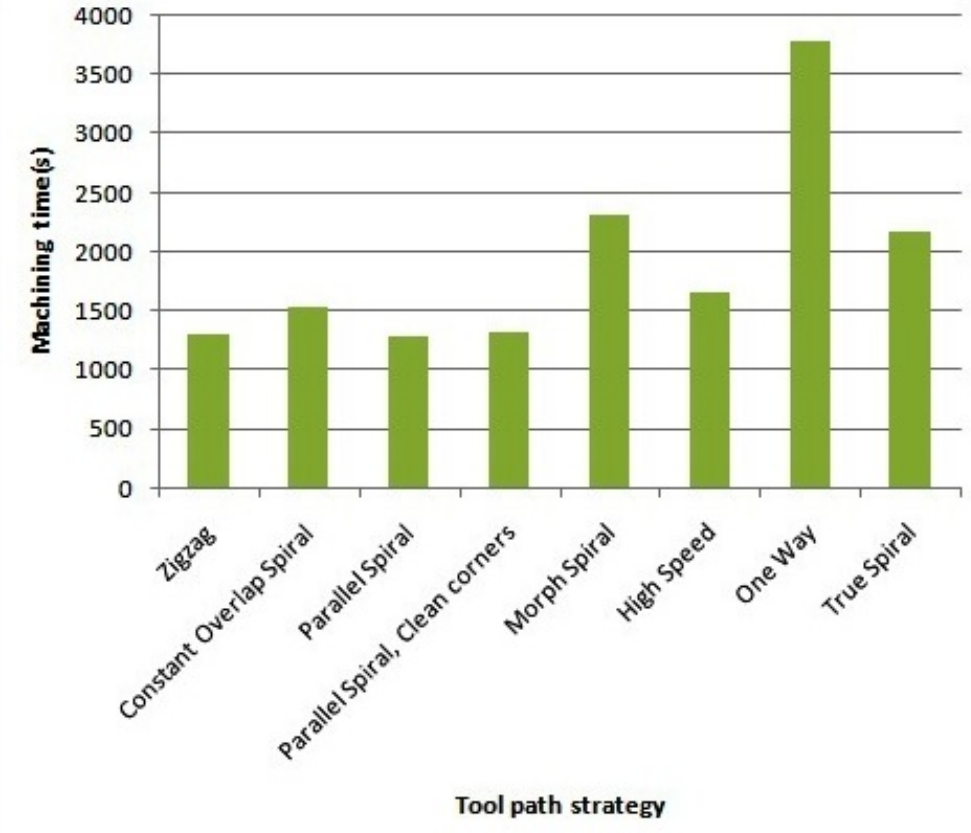

Figure 3.8. Machining times when using different tool path strategies (Rectangular pocket, 30 mm by 20 mm by 10 mm)

3.4.2 Fixture and workpiece design and preparation

To be able to mount the workpiece securely onto the dynamometer, a fixture was designed and machined. The design was such that there was a provision to fasten the workpiece onto the fixture and also secure the fixture-workpiece assembly onto the dynamometer. The workpiece was fastened onto fixture using four M12 socket bolts and the fixture-workpiece assembly was secured onto dynamometer using six M10 socket bolts.

3.4.3 Dynamometer calibration

The setup used in dynamometer calibration is illustrated in Figure 3.9.

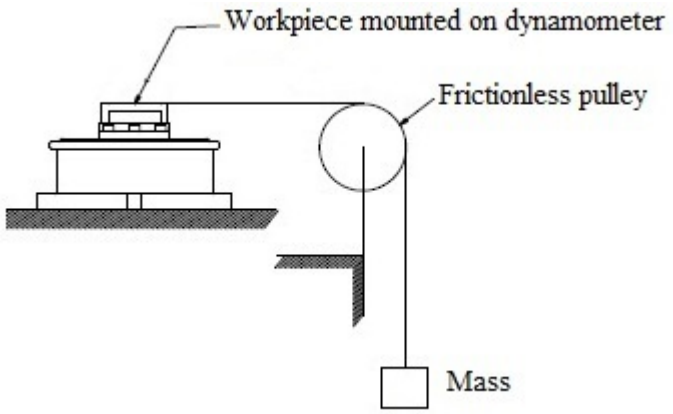

Figure 3.9. Experimental setup for dynamometer calibration

Loads of known weights were applied along the x and y direction one at a time and the readings in all 3 components were recorded. It was observed that for each direction loaded there was interaction in all 3 components which was compensated for by the use of calibration equations. Calibration curves were obtained for 3-component cutting force dynamometer, from which the force components for all directions were derived.

3.4.4 Verification of cutting force models

The experimental verification of models and machining work was done on a Fanuc Series Oi-MD machining center using 2-flute and 4-flute HSS helical end mills with a diameter of 8mm. A schematic of the experimental setup is shown in Figure 3.10 and a photograph of the actual setup in Figure 3.11.

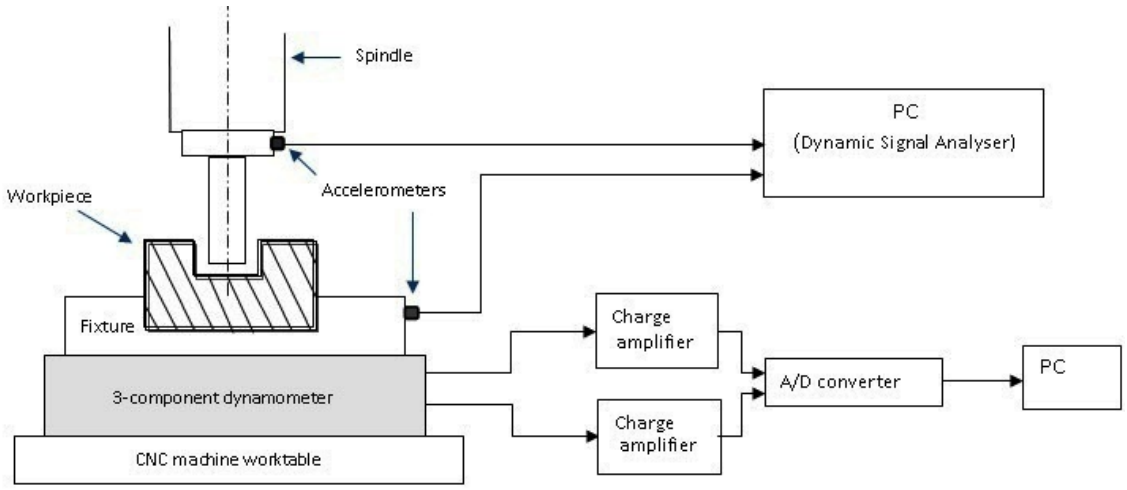

Figure 3.10. Experimental setup

The workpieces material was Aluminium alloy 7075A, which is often used in manufacture of aerocraft and other aerospace components. Pocket profiles were drawn and tool paths generated using Mastercam X6 software. These were transferred to the CNC machine via ethernet connection using TYP Soft FTP server software.

The cutting force and vibration measurement system is comprised of LabVIEW software, the data acquisition system, which is a NI-DAQ card model USB-6008 and the measuring devices (sensors), in this case, piezoeletric dynamometer for the cutting force measurement and piezoelectric accelerometers model AC-102 for vibration measurement.

The measurement and data acquisition system comprises of a dynamometer ,

two accelerometers model AC-102, three charge amplifiers, an NI-DAQ card USB 6008, LabView software and the relevant connecting cables. As the tool cuts through the workpiece, the force is transmitted to the dynamometer. Cutting force measurements were taken using a table mounted dynamometer during machining. The dynamometer measures the cutting force in the x, y and z axes. The dynamometer is clamped between the workpiece and the table. The fixture was used to mount the workpiece on the dynamometer. When the piezoelectric quartz in the dynamometer is strained an electric charge is generated. The electric charge is then transmitted to the charge amplifiers through the connecting cable where it is amplified. The voltage output by amplifier corresponds to the cutting force based on the parameters set in the charge amplifier.

The accelerometers were mounted on the workpiece to measure vibration in the x and y directions, using threaded studs which provided a firm mounting.

The DAQ card transmits the voltage signals from the charge amplifiers and the accelerometers into a PC via USB slot so that the LabVIEW software is able to read and utilize the data.

3.5 Chatter stability criterion

A set of experiments and signal analysis were carried out in order to set a chatter value. This value is the ratio of maximum predicted cutting force to maximum predicted static cutting force. Since the measured cutting force is in agreement with predicted dynamic cutting force, the chatter element allows chatter prediction without the need for experiments.

Chatter vibration was not clearly evident in the cutting force waveforms, since the workpiece material is soft. Therefore, the vibration signals from the accelerome-

Figure 3.11. Photograph of the experimental setup

ters were analyzed in the frequency domain. In the frequency spectrum, chatter is present when there are large peaks near the natural frequency of the system. A stable cut only has peaks due to resonance at natural frequency and tooth passing frequency in the frequency spectrum. In the frequency spectrum for an unstable cut other frequency peaks are observed within the range of 20-27 Hz, which are the vibration frequencies.

A digital low-pass filter was applied to the accelerometer data signal to minimize high frequency noise signal which was observed. The data processing was done in MATLAB®.

For example in a pocket milling test at spindle speed 450 rpm, axial depth of cut 1 mm, feedrate 0.08 mm/tooth using a cutter of diameter 8 mm, the maximum static and dynamic forces were found to be 16.48 N and 19.03 N respectively, giving a ratio ρ of 1.154.

$$F_{dy}\,\max = -19.03 \text{ N}$$

$$F_{st}\,\max = -16.48 \text{ N}$$

$$\rho = \frac{F_{dy}\,\max}{F_{st}\,\max} = 1.154,$$

where F_{dy} max is Maximum dynamic cutting force and F_{st} max is maximum static cutting force.

The FFT of vibration for this milling test is shown in Figure 3.5.

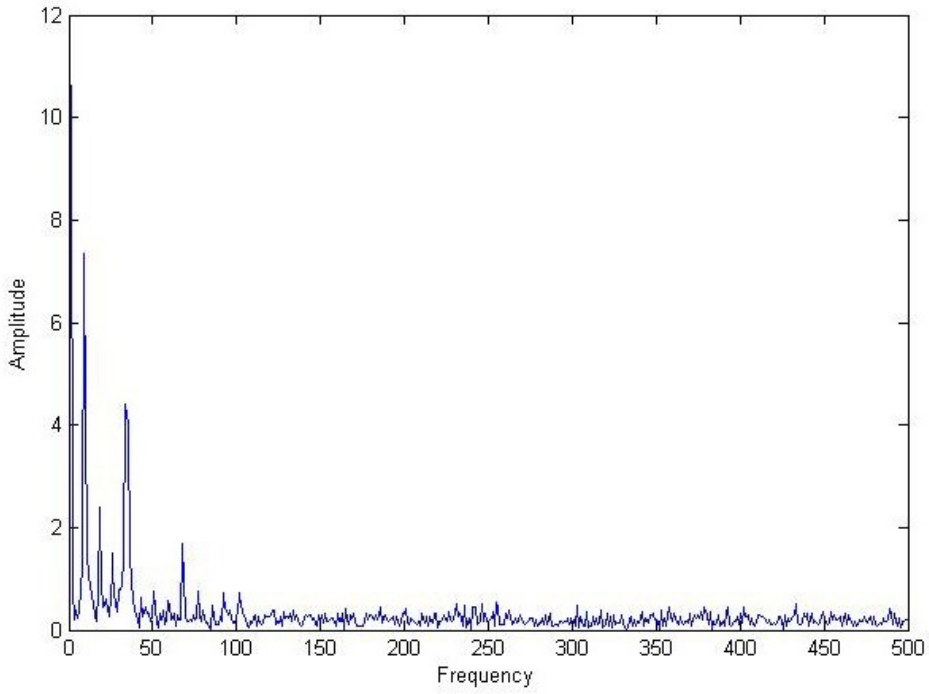

Figure 3.12. Frequency spectrum (f=0.08, a=0.5 mm, N=450 rpm)

When chatter occurs, the increase in vibration levels is reflected in the acceleration signals. With this ratio, the occurrence of chatter can be avoided during actual machining by optimizing the milling parameters to provide a ratio of less than the ratio $/rho$ for the cutter-worpiece combination, while maintaining maximum material removal rate.

3.6 Optimization of pocket milling parameters

The goal of optimization in this research is to select process parameters that ensure minimal cutting forces, ensure chatter vibration does not occur, while taking the shortest time possible to machine a pocket. Being a multi-objective optimization problem, the weighted sum optimization approach was applied. This method scales the set of objectives into a single objective by multiplying each objective with its respective weight [39]. This is formulated as

$$A_i = \sum_{j=1}^{n} w_i a_i \tag{3.14}$$

where a_1 is force ratio below 1.238, a_2 is minimum cutting force and a_3 is minimum machining time, and $w_1 = 5$ for a_1, and $w_1 = 3$ for a_2, and $w_1 = 2$ for a_3.

The static and dynamic force models are used to determine the prediction of chatter vibration occurrence. Mastercam® software is used to simulate and store machining times, which are read by optimization algorithm. The parameters under study are feedrate and axial depth of cut. The algorithm allows off-line optimization of the machining parameters especially the feedrate based on the predicted cutting force, chatter value and machining time. MATLAB® software was used to develop the optimization algorithm whose summary is shown in Figure 3.6.

The integration of the models developed in the simulation of the pocket milling process including the tool path strategy was not achieved due to limitations in the softwares used, that is MATLAB® and Mastercam®. Such work done from a single platform such as Matlab is possible but could not be accomplished within the research period. The development of a platform for simulation of the milling process with consideration of the tool path strategy is thus a potential research

area.

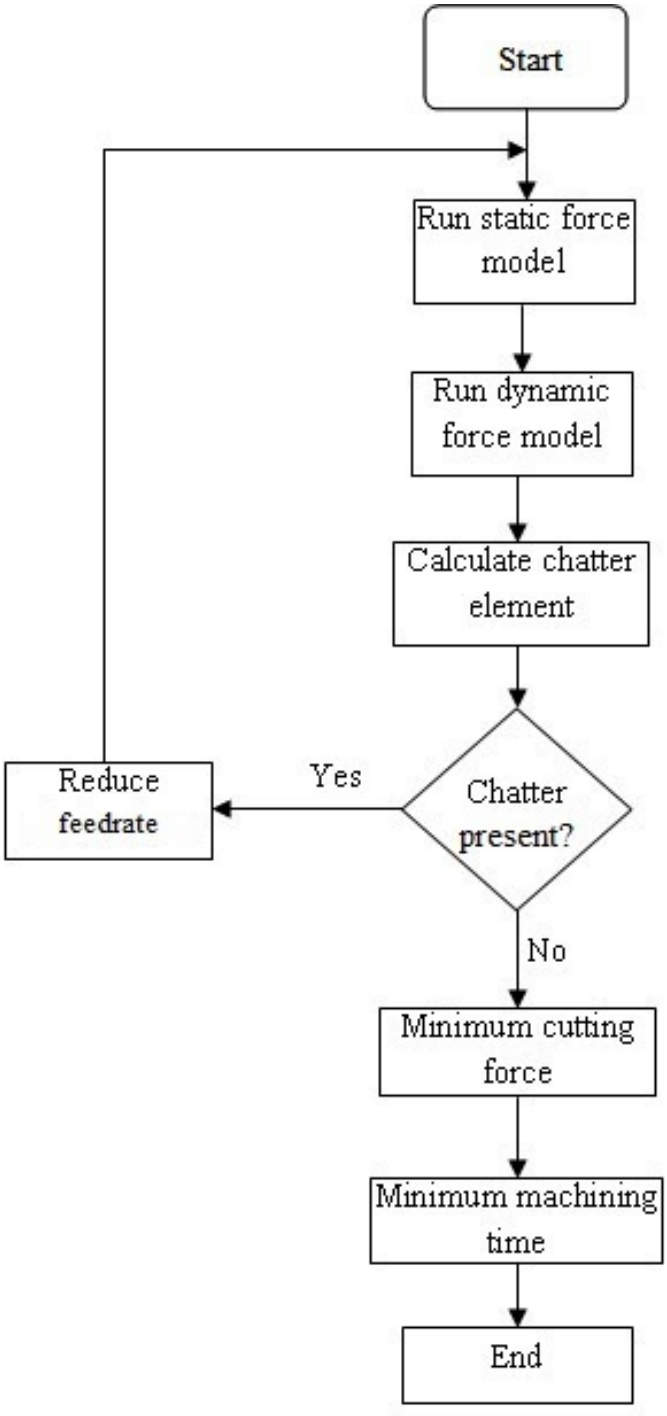

Figure 3.13. Optimization flowchart

CHAPTER 4

RESULTS AND DISCUSSION

In this chapter, results on cutting constants determined using the mechanistic approach are presented. Also, experimental results verifying the developed models, and results on the effects of pocket milling parameters on milling forces and chatter vibration are presented and discussed. The parameters investigated include axial depth of cut, feedrate and tool path strategy.

4.1 Determination of cutting constants

Figure 4.1 shows a waveform of measured instantaneous cutting force.

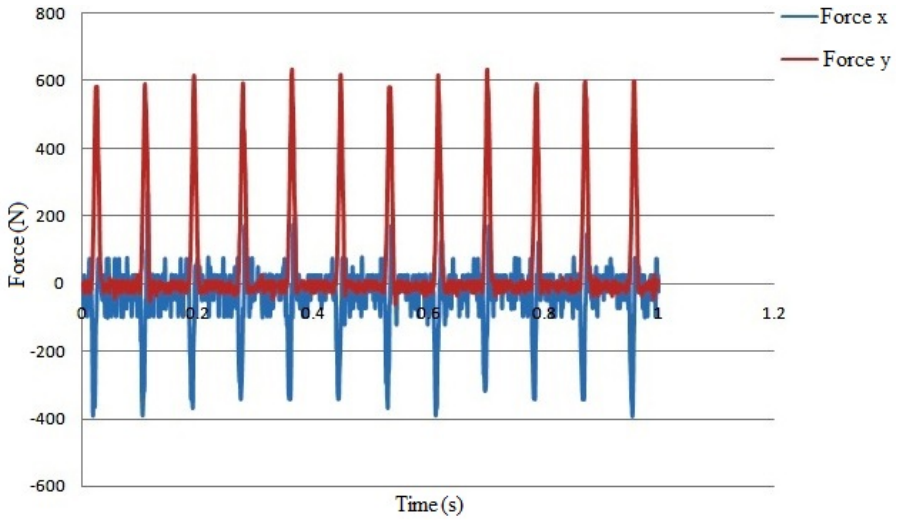

Figure 4.1. Force waveforms for side milling (f=0.2 mm/t, N=705 min^{-1},a= $5mm$,$\mathbf{n}_t$=1)

From this kind of waveform, the average cutting forces per tooth period for the different feedrates were obtained as given in Table4.1. These values are applied in Equation 2.18 and the cutting and edge force coefficients obtained are given in Table 4.2.

Table 4.1: Average cutting forces per tooth period

Feedrate	$\overline{F}_x$**(N)**	$\overline{F}_y$**(N)**	$\overline{F}_z$**(N)**
0.1	-19.5	72.5	-21.6
0.2	-23.2	135.4	-30.2
0.3	-34.5	160.2	-35.8
0.4	-36.2	224.1	-41.4

Table 4.2: Cutting and edge coefficients

Constant	Symbol	Value
Tangential cutting coefficient	K_{tc}	198.4
Radial cutting coefficient	K_{rc}	90.63
Axial cutting coefficient	K_{ac}	890
Tangential edge coeffcient	K_{te}	30.86
Radial edge coefficient	K_{re}	17.96
Axial edge coefficient	K_{ae}	-7.89

4.2 Verification of static and dynamic cutting force models

Experimental tests were carried out to verify the static and dynamic force models that were developed. For this tests, the standard milling parameters were as in Table4.3.

Table 4.3: Standard milling parameters

Parameter	**Value**
Number of teeth	4
Cutter overhang length	30 mm
Axial depth of cut	1 mm
Feedrate	0.08 mm/tooth
Spindle speed	450rpm
Tool path strategy	Parallel spiral

Figure 4.2 shows the waveforms of instantaneous cutting forces from measured and predicted forces in x and y directions, respectively.

It can be seen from this waveforms that the predicted forces are generally in good

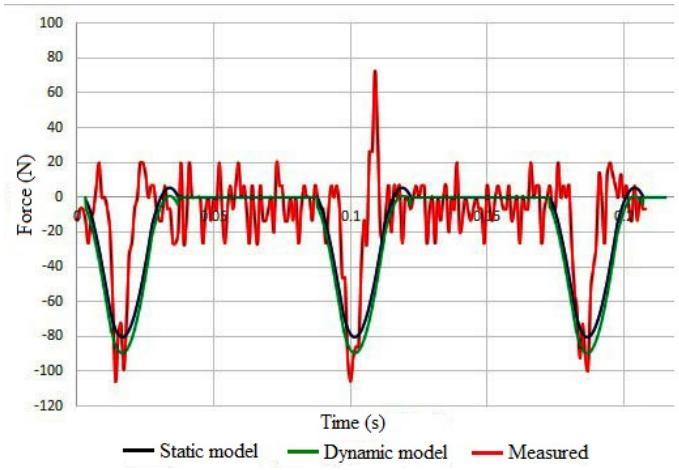

(a) Force in x direction

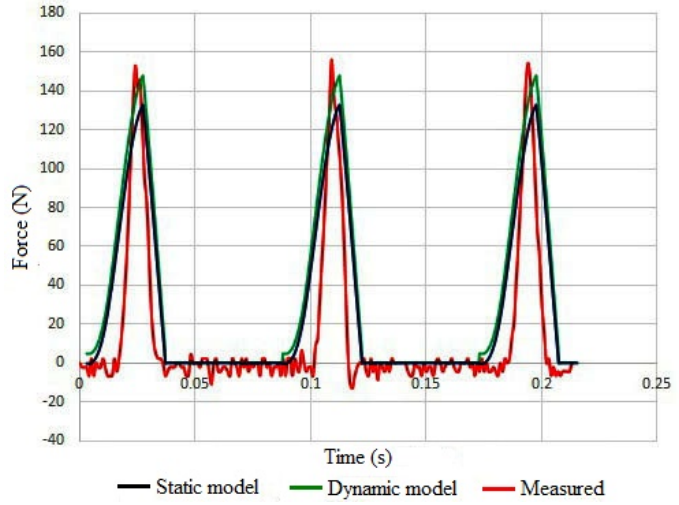

(b) Force in y direction

Figure 4.2. Waveforms for predicted and measured cutting forces

agreement with experimental results. The measured signal has noise disturbances unlike both static and dynamic models, which is due to the engagement and disengagement of the cutting tool from the workpiece. This noise signal is more pronounced in the x direction, which was the feed direction for this test. This is because the greatest tool displacements occur in the feed direction. The dynamic model is found to be more accurate than the frequently used static model. The average percentage error when predicting using static model was found to be 16.86% while the average percentage error when using dynamic force model was

7.98% as obtained in Table 4.4. The dynamic model is thus more reliable.

Table 4.4: Table of comparison for measured and predicted forces

Test	Average experimental resultant force(N)	Static model average resultant force	Percentage error	Dynamic model average resultant force	Percentage error
1	14.27	15.90	11.46	12.94	9.32
2	35.46	38.72	9.20	37.95	7.02
3	51.52	63.12	22.52	57.38	11.38
4	91.38	96.76	5.89	96.26	5.34
5	44.30	49.85	12.54	43.15	2.60
6	74.26	87.41	17.71	73.26	1.35
7	87.93	96.76	10.04	80.06	8.95
8	23.02	24.41	6.06	24.55	6.66
9	58.84	68.54	16.48	65.21	10.83
10	53.39	59.80	12.00	55.17	3.34
11	61.56	81.03	31.63	65.24	5.99
12	36.79	46.14	25.43	31.91	13.26
13	35.96	41.28	14.82	39.17	8.93
14	100.07	111.05	10.97	101.25	1.18
15	157.25	170.14	8.20	126.21	19.74
16	132.73	136.66	2.96	133.03	0.23

4.3 Effect of depth of cut on cutting force

Test were done at varying depths of cut, with all other parameters maintained at standard values given in Table 4.3. The data obtained is given in Table 4.5. It was observed that cutting forces increased with increase in depth of cut and decreased with decrease in depth of cut, as shown in Figure 4.3 in x and y direction. As axial depth of cut increases, the area of contact of the tool with the workpiece, and the volume of material removed also increase, which leads to increase in cutting force. The predicted values were in good agreement with the measured values.

Depth of cut (mm)	Predicted F_x (N)	Predicted F_y (N)	Measured F_x (N)	Measured F_y (N)
0.5	-11.91	16.26	-14.30	18.22
1	-23.83	32.53	-26.21	32.20
1.5	-35.74	48.79	-35.74	49.77
2	-47.65	65.06	-50.04	67.01

Table 4.5: Variation of cutting force with depth of cut

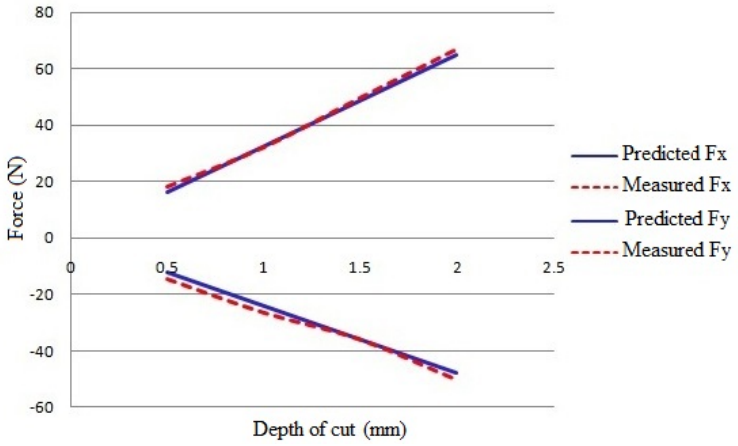

Figure 4.3. Variation of cutting force with depth of cut

4.4 Effect of feedrate on cutting force

Test were done at varying feedrates, with all other parameters maintained at standard values given in Table 4.3. The data obtained is given in Table 4.6. Cutting forces increase with increase in feedrate and decrease with decrease in feedrate, as shown in Figure 4.4. Higher feedrate increases the material remove rate (MRR) which results in higher cutting forces. Also with high feedrate the metal may be pushed instead of being cut. This also results in higher cutting force and higher temperature. The predicted values were in good agreement with the measured values.

Feedrate (mm/tooth)	Predicted F_x (N)	Predicted F_y (N)	Measured F_x (N)	Measured F_y (N)
0.02	-14.68	11.05	-14.97	11.27
0.08	-23.83	32.53	-21.69	29.60
0.14	-31.65	43.68	-28.09	39.56
0.2	-39.73	59.47	-44.50	66.61

Table 4.6: Variation of cutting force with feedrate

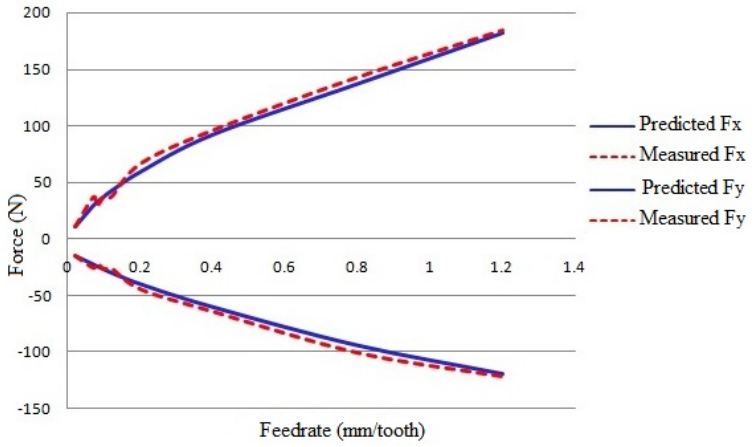

Figure 4.4. Variation of cutting force with feedrate

4.5 Cutting force waveforms for different tool path strategies

The cutting force waveforms observed when milling using parallel spiral tool path, zigzag tool path and true spiral tool path are shown in Figure 4.5. The measurement time period is one complete depth pass. The cutter parameters were $D = 8$ mm, $n_t = 4$, overhang length=30 mm. The milling parameters for all three tests were: $a = 0.5$ mm, $f = 0.07$ mm/tooth, $N = 500$ rpm.

The peak-to-peak force when milling using true spiral tool path is 125.26 N in the x direction and 143.60 N in the y direction. When milling using parallel spiral tool path the peak-to-peak force in x direction is 203.72 N and 206.79 N

in the y direction. The highest peak-to-peak forces occur when using zigzag tool path with force in x direction being 173.17 N in x direction and 254.73 N in y direction. The highest force values are measured at corner sections of the milling path, where there is larger tool engagement into the workpiece.

From the analysis, it was observed that the tool path strategy used had a significant effect on the magnitude of cutting forces that the tool experiences. Rapid direction changes caused a rise in cutting forces, due to the variation of the extent of radial engagement of the cutting tool as its direction changes. At the corner sections seen in zigzag and parallel spiral tool path, the maximum radial engagement of the tool occurs. The true spiral tool path, where the tool does not make sharp direction changes has the least average cutting forces in both directions.

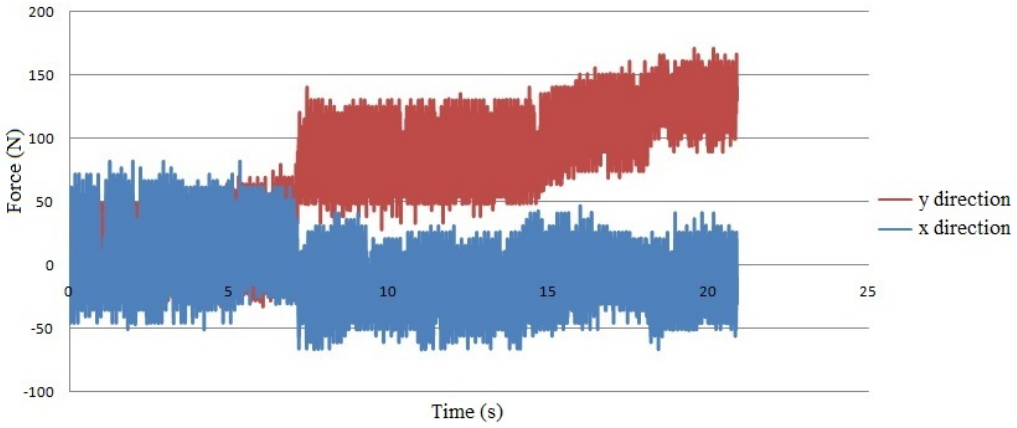

(a) Parallel spiral

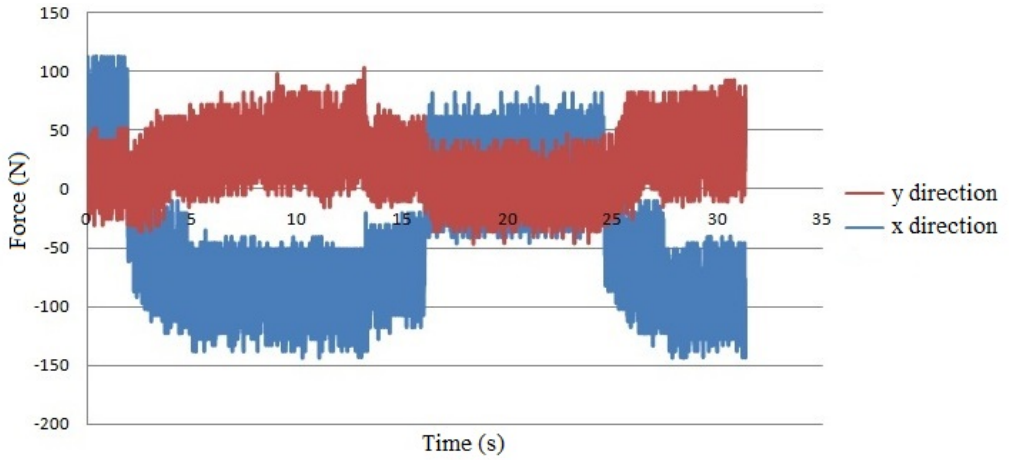

(b) Zig-zag

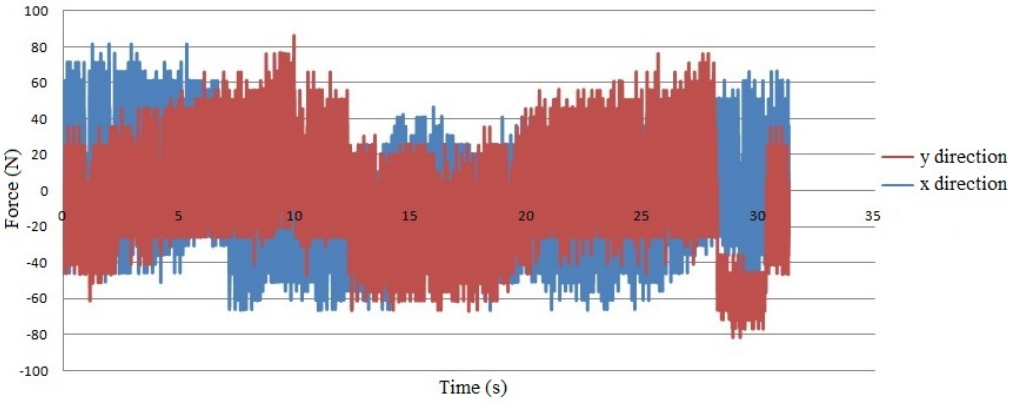

(c) True spiral

Figure 4.5. Cutting force waveforms for various tool path strategies

4.6 Effect of tool path strategy on cycle time

Milling tests were done to machine two pockets, a square of length 30 mm and a rectangular pocket measuring 40 mm by 30 mm. The machining time for milling the rectangular pocket using parallel spiral tool path was 670 seconds, with zigzag tool path was 636 seconds while using true spiral tool path was 874 seconds. The machining time for milling the square pocket using parallel spiral tool path was 338 seconds, with zigzag tool path was 301 seconds while using true spiral tool path was 291 seconds as shown in Figure 4.6.

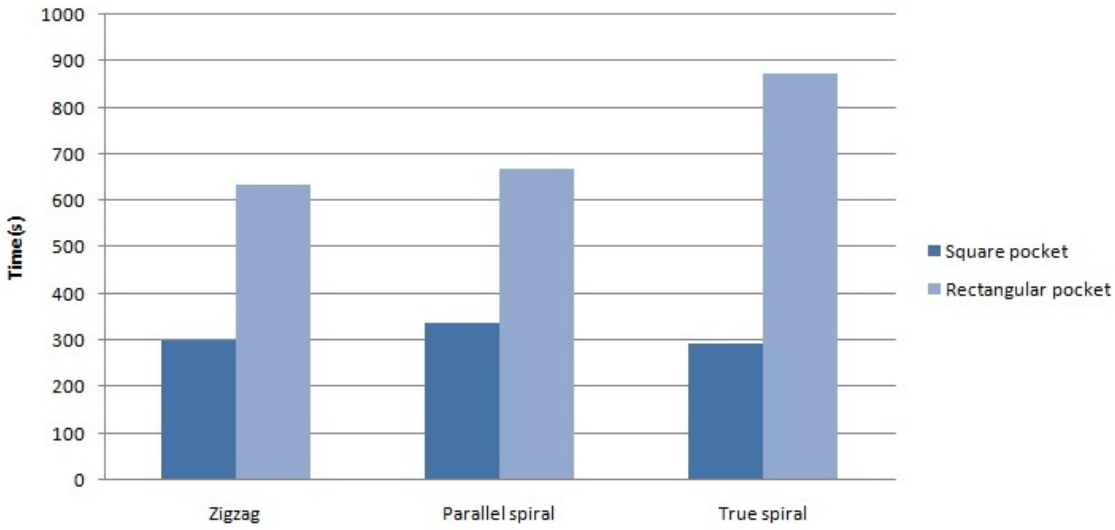

Figure 4.6. Cycle times for different tool path strategies

The suitability of a tool path strategy in terms of cycle time is dependent on the profile of the pocket. For the rectangular pocket, zigzag tool path strategy took the shortest to machine the pocket while true spiral took the longest time. For the square pocket, true spiral tool path strategy took the shortest time while parallel spiral tool path took the longest time.

4.7 Determination of chatter boundary

In order to determine the force ratio, a set of experiments were conducted with depth of cut, feedrate and spindle speed being varied. The vibration signals from the accelerometers were analyzed in the frequency domain. In the frequency spectrum, chatter is present when there are large peaks near the natural frequency of the system. A stable cut only has peaks due to natural frequency and tooth passing frequency in the frequency spectrum. Tests with this kind of spectrum are plotted as ○ in Figure 4.7.

In the frequency spectrum for an unstable cut , plotted as ●, other frequency peaks are observed within the range of 20-27Hz, which are the vibration frequencies. This can be seen in Fig. 10(d). Test for which there are other small peaks which cannot be concluded to be chatter, such as in Fig. 10(c) are plotted as ◑.

Table 4.7 shows the values of ρ obtained for 20 tests. These data was plotted as shown in Figure 4.7, from which a boundary was observed at 1.238.

Test	Force ratio	Vibration
1	1.114	no
2	1.280	yes
3	1.209	slight
4	1.326	yes
5	1.165	slight
6	1.138	no
7	1.127	no
8	1.154	no
9	1.248	yes
10	1.223	slight
11	1.105	no
12	0.992	no
13	1.249	yes
14	1.302	yes
15	1.042	no
16	1.273	yes
17	1.626	yes
18	1.238	yes
19	1.158	slight
20	1.120	no

Table 4.7: Table of force ratios

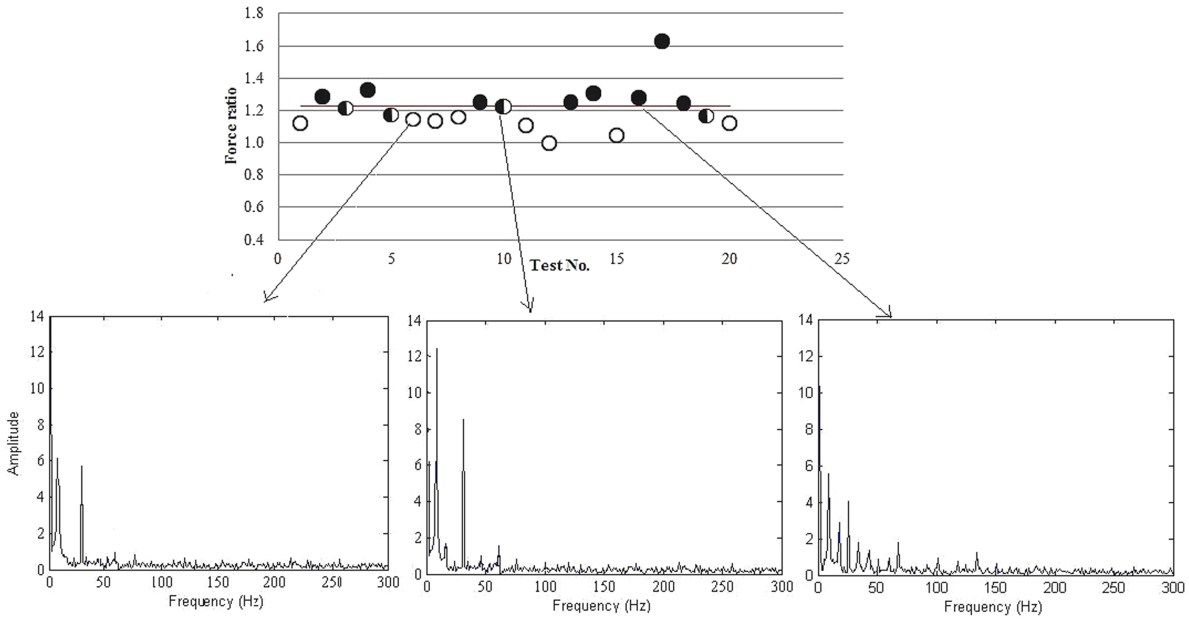

Figure 4.7. Plot of chatter values

During milling, parameters can be selected and applied in the chatter prediction model, where the ratio of maximum dynamic cutting force to maximum static cutting force is evaluated. For the cutter-workpiece combination used in this experiment, a ratio equal to or above 1.238 means that chatter vibration is expected to occur.This force ratio was successfully applied to predict, and thus avoid, occurrence of chatter vibrations.

4.8 Effect of tool path strategy on chatter vibration

The cutting force and vibration data measured in time domain was transformed into frequency domain using Fast Fourier Transform (FFT) method. This transformation was done in order to identify occurrence of chatter vibrations during

milling. From the FFT analysis it is observed that the forces are harmonic waves. The dominant peak frequency occurred at 30 Hz, which is the tooth passing frequency. Harmonics of the fundamental frequency which occur at integral multiples of the fundamental frequency are also observed in some experiments. A peak due to the spindle frequency was also observed at 7.5Hz. The variation in magnitudes of fundamental frequency from the performance of an FFT analysis can be used as an indicator to detect the variations of the cutting force [40].

FFT analysis was done on force measured when machining a pocket at standard machining parameters given in Table 4.3 using parallel spiral tool path, zigzag tool path, and true spiral tool paths. The chatter prediction model gives a chatter value of 0.736, hence chatter vibration was not predicted to occur. The frequency spectrum of the measured forces is shown in Figure 5.1. There was no chatter for any of the tool path strategies used. The tooth passing frequency for both tests is 30 Hz, which is observed as the fundamental frequency in all three tests.

Since standard parameters did not present chatter vibration, the feedrate was increased to 0.125 while all other parameters were maintained. This gave a force ratio of 1.248, hence chatter vibration was predicted to occur. The FFT plots are shown in Figure 4.8. The tooth passing frequency for both tests is 30 Hz, which is observed as the fundamental frequency in all three tests.

From the FFT analysis, chatter vibration occurred during machining with all three tool path strategies, as explained in Section 4.5. The tool path strategy was not observed to affect the occurrence or lack of chatter vibration from the FFT spectrum of vibration signal. However, the RMS of vibration acceleration was observed to vary slightly with similar milling parameters but different tool path strategy. This is due to the effect of sudden direction changes during machining of corners in parallel spiral and zigzag tool paths.

The vibrations had the higher RMS when using parallel spiral tool path and were not fully developed when using true spiral tool path. Force variations only occurred at the end of the machining cycle for true spiral tool path, when the tool encountered corner cutting.

4.9 Variation of vibration with feedrate

Pocket milling tests were carried out at standard parameters given in Table 4.3, except feedrate which was varied of between 0.05 mm/tooth and 1.11 mm/tooth. The frequency spectrum of the vibration measurements were analyzed and the results compared. The severity of vibration is observed from the height of the peaks at the various frequencies. At a high feedrate of 1.11 mm/tooth, the dominant frequency shifts to the vibration frequency observed between 22-25 Hz as seen in Figure 4.9. This is as a result of increased load on the teeth of the cutter at higher feedrates, which is also transmitted to the workpiece.

In this chapter, the variation of machining time with various tool path strategies was presented and discussed. The zigzag tool path strategy was found to have the least machining time for the rectangular pocket profile while the true spiral tool path was found to present the least machining time for a rectangular pocket.

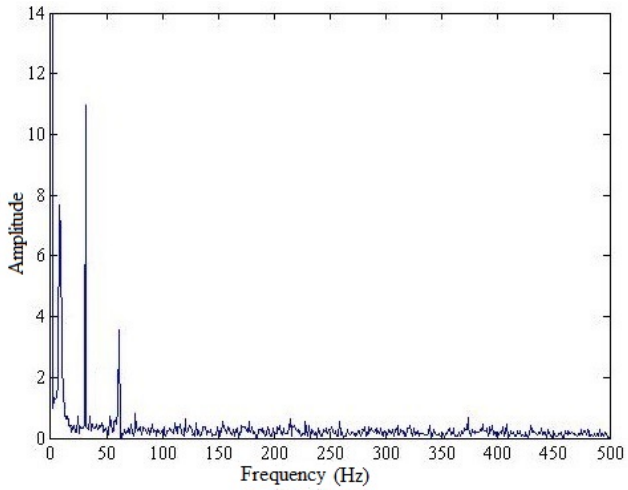

(a) Parallel spiral:no chatter vibration

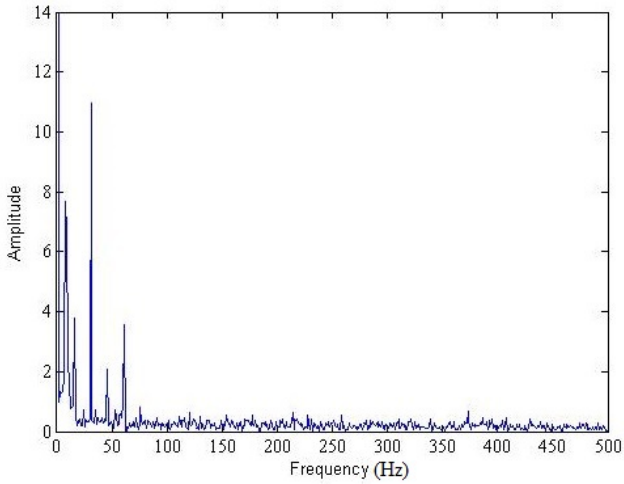

(b) Zigzag: no chatter vibration

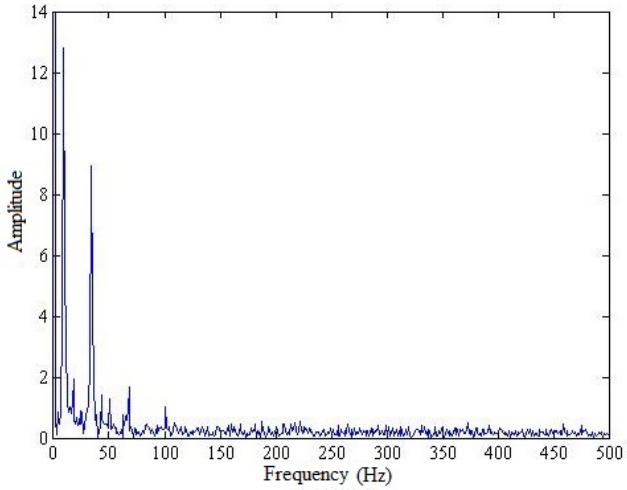

(c) True spiral: no chatter vibration

Figure 4.8. Effect of tool path strategy on chatter occurrence

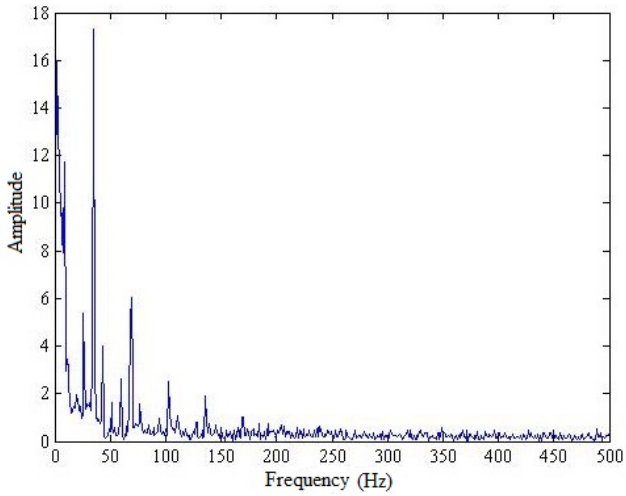

(a) Parallel spiral:chatter vibration present

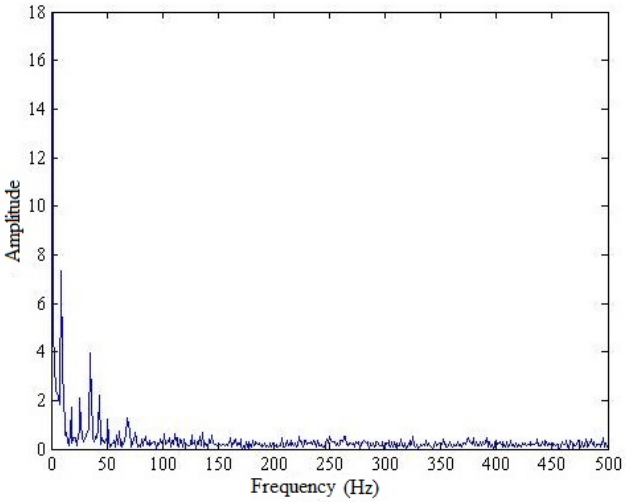

(b) Zigzag: chatter vibration present

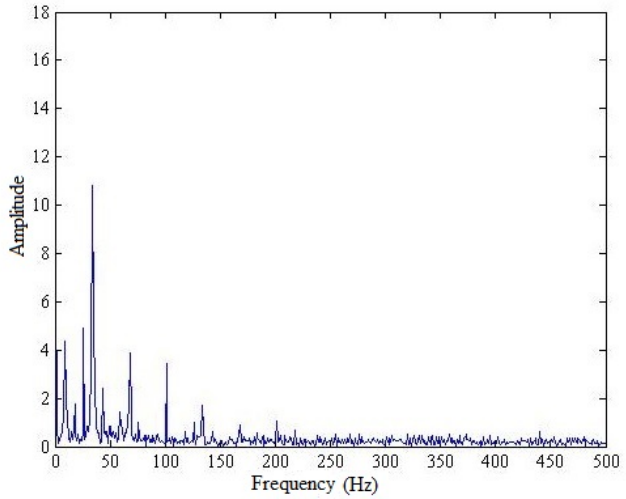

(c) True spiral: chatter vibration present

Figure 4.9. Effect of tool path strategy on chatter vibration

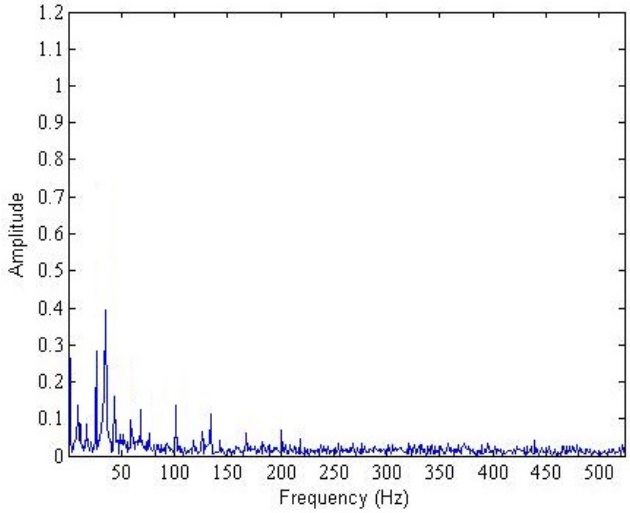

(a) 0.05 mm/tooth

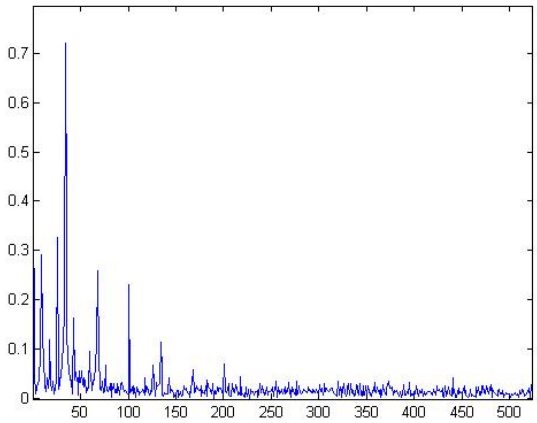

(b) 0.83 mm/tooth

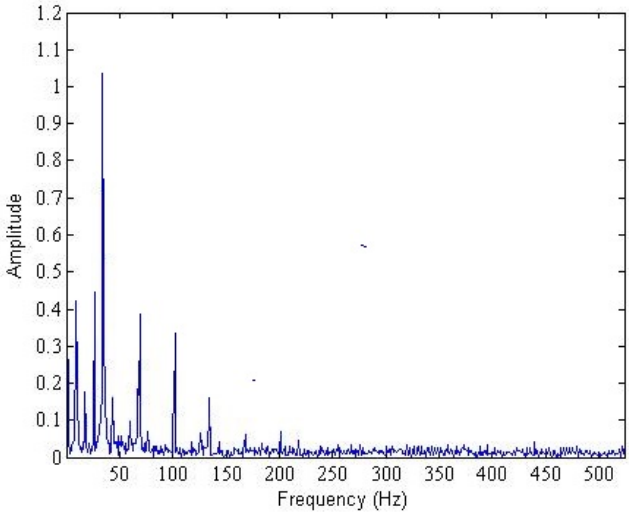

(c) 1.11 mm/tooth

Figure 4.10. Frequency analysis of vibration at different feedrates

CHAPTER 5

CONCLUSION AND RECOMMENDATIONS

5.1 Conclusion

In this study, static and dynamic force models for pocket milling were developed and validated. The models developed were tested at various depths of cut, feedrate and using various tool path strategies.

These models were applied to predict chatter vibrations for the pocket milling process. A chatter indicator defined as the ratio of dynamic force to static force was validated through experimental work. It was established that for the machining of aluminium alloy 7075 using the HSS cutting tool this force ratio is 1.238.

An optimization control algorithm implemented in MATLAB® was developed to establish the optimal combination of parameters for milling of a pocket. With a given set of milling parameters, the occurrence of chatter could be predicted and hence avoided by adjusting the depth of cut and feedrate. The depth of cut, feedrate and tool path strategy on the occurrence of chatter vibration was also investigated. It was not possible to change the tool path strategy within the optimization algorithm due to incompatibility between the MasterCAM® software and MATLAB®. The algorithm was verified using experiments and was found to be effective in ensuring chatter avoidance during actual milling.

5.2 Recommendations

Dynamics and stability modelling of milling process can influence various industrial applications such as aerospace, automotive, die and mould, toolings, robots, precision machining. From this study the following are recommendations towards improvement in this area:

1. Incorporation of force and chatter prediction model in tool path generation during pocket milling, to enable change of small sections of tool path to suit the pocket profile. This is more for pockets with complex profiles.

2. The models developed cannot accurately predict the forces in corner cutting during pocket milling. An adaptive controller should thus be developed that can prevent the sharp rises in cutting force in such conditions.

REFERENCES

[1] D. M. Sukru, *Mechanics and Dynamics of Serrated End Mills.* PhD thesis, University of British Columbia, 2003.

[2] B. W. Ikua, H. Tanaka, O. Fumio, and S. Satoshi, "Prediction of cutting forces and machining error in ball end milling of curved surfaces-I Theoretical analysis," *Journal of International Society for Precision Engineering and Nanotechnology*, vol. 25, 2002.

[3] M. Held, *On the Computational Geometry of Pocket Machining.* Springer Science-Verlag, 1991.

[4] T. R. Kramer, "Pocket Milling with Tool Engagement Detection," *Journal of Manufacturing Systems*, vol. 11, pp. 114–123, 1992.

[5] G. Quintana and J. Ciurana, "Chatter in machining processes: A review," *International Journal of Machine Tools and Manufacture*, vol. 51, pp. 363–376, may 2011.

[6] S. Fishwick and W. Tobias, "A theory of Regenerative Chatter," *The Engineer-London*, 1958.

[7] H. S. Choy and K. W. Chan, "A corner-looping based tool path for pocket milling," *Computer-Aided Design*, vol. 35, pp. 155–166, 2001.

[8] S. Park and B. Choi, "Tool-path planning for direction-parallel area milling," *Computer-Aided Design*, vol. 32, no. 1, pp. 17–25, 2000.

[9] A. E. M., M. Held, and C. L. Smith, "Optimization problems related to zigzag pocket machining," *Algorithmica*, vol. 26, no. 2, pp. 197–236, 2000.

[10] Advanced Robotic Technology, "Optimum tool path strategies reduce production times," 2011.

[11] P. N. Rao, *Manufacturing Technology: Metal Cutting and Machine Tools*. Tata McGraw-Hill Plublishing Company Limited, 2 ed., 2009.

[12] B. W. Ikua, H. Tanaka, F. Obata, S. Sakamoto, T. Kishi, and T. Ishii, "Prediction of cutting forces and machining error in ball end milling of curved surfaces -II experimental verification," *Precision Engineering*, vol. 26, no. 1, pp. 69–82, 2002.

[13] J. G. Njiri, *Optimization of machining process for freeform surfaces using an intelligent adaptive controller (M. Sc. Thesis)*. 2010.

[14] J.-W. Dang, W.-H. Zhang, Y. Yang, and M. Wan, "Cutting force modeling for flat end milling including bottom edge cutting effect," *International Journal of Machine Tools and Manufacture*, vol. 50, no. 11, pp. 986–997, 2010.

[15] J. J. Wang, "Convolution Analysis of Milling Force Pulsation," *Journal of Engineering for Industry*, vol. 116, no. 25, 1994.

[16] O. Omar, T. El-Wardany, E. Ng, and M. Elbestawi, "An improved cutting force and surface topography prediction model in end milling," *International Journal of Machine Tools and Manufacture*, vol. 47, pp. 1263–1275, jun 2007.

[17] W. Kline, R. Devor, and J. Lindberg, "The prediction of cutting forces in end milling with application of cornering cuts," *International Journal of Machine Tool Design and Research*, vol. 22, no. 1, p. 722, 1982.

[18] Y. Altintas, *Manufacturing Automation: Metal Cutting Mechanics, Machine Tool Vibrations, and CNC Design.* Cambridge University Press, 2012.

[19] E. Budak, Y. Altintas, and E. Armarego, "Prediction of milling force coefficients from orthogonal cutting data.," *Journal of Manufacturing Science and Engineering*, vol. 118, no. 2, pp. 216–224, 1996.

[20] R. Butt, *Introduction to Numerical Analysis Using MATLAB*. Jones and Bartlett Publishers, 2009.

[21] C. W. de Silva, *Vibration and Shock Handbook*. CRC Press, 2005.

[22] J. Tlusty and F. Ismail, "Basic non-linearity in machine chatter," *Annals of CIRP*, vol. 30, no. 1, pp. 21–25, 1981.

[23] J. Tlusty and P. Macneil, "Dynamics of cutting forces in end milling," *Annals of the CIRP*, vol. 24, pp. 21–25, 1975.

[24] J. H. Ko and Y. Altintas, "Time domain model of plunge milling operation," *International Journal of Machine Tools and Manufacture*, vol. 47, no. 9, 2007.

[25] R. L. Allen and D. W. Mills, *Signal Analysis: Time, Frequency, Scale, and Structure*. John Wiley & Sons, 2004.

[26] J. H. Ko and K. C. Shaw, "Chatter prediction based on frequency domain solution in CNC pocket milling," *International Journal of Precision Engineering and Manufacturing*, vol. 10, no. 4, pp. 19–25, 2009.

[27] L. T. Taner, S. Matej, and K. Jan, "Integrated simulation system for 5-axis milling cycles," in *15th C IRP Conference on Modelling of Machining Operations*, 2015.

[28] P. Palpadian, R. V. Prabhu, and B. S. Satish, "Stability Lobe Diagram for High Speed Machining Process:Comparison of Experimental and Analytical Methods A Review," *International Journal of Innovative Research in Science, Engineering and Technology*, vol. 2, no. 3, 2013.

[29] S. Daneshmand, M. M. Abdolhosseini, and C. Aghanajafi, "Investigating the Optimal Tool Path Strategies Based on Machining Time in CAD-CAM," *Australian Journal of Basic and Applied Sciences*, vol. 5, no. 12, pp. 2320–2326, 2011.

[30] L. López de Lacalle, A. Lamikiz, J. Sánchez, and M. Salgado, "Toolpath selection based on the minimum deflection cutting forces in the programming of complex surfaces milling," *International Journal of Machine Tools and Manufacture*, vol. 47, no. 2, pp. 388–400, 2007.

[31] S. Choi and H. Cheung, "A topological hierarchy based approach to tool path planning for multi-material layered manufacturing," *Computer-Aided Design*, vol. 38, pp. 143–156, 2006.

[32] M. Korosec and J. Kopac, "Neural Network Based Selection of Optimal Tool - Path in Free Form Surface Machining," vol. 1, no. December, 2007.

[33] H.-C. Kim, "Tool path modification for optimized pocket milling," *International Journal of Production Research*, vol. 45, no. 24, pp. 5715–5729, 2007.

[34] T. El-midany, H. Tawfik, and A. Elkeran, "Tool path pattern comparison: Contour parallel with Direction-parallel," in *International Conference on Geometric Modeling and Imaging-New Trends*, 2006.

[35] M. Bouard, V. Pateloup, and P. Armand, "Pocketing toolpath computation using an optimization method," *Computer-Aided Design*, vol. 43, no. 9, pp. 1099–1109, 2011.

[36] S. J. Wang, S. To, X. Chen, X. D. Chen, and X. B. Ouyang, "An integrated optimization of cutting parameters and tool path generation in ultraprecision raster milling," *The International Journal of Advanced Manufacturing Technology*, vol. 75, no. 9, 2014.

[37] X. Li, Q. Wang, J. Zhang, and J. Liu, "Tool path optimization for energy efficient machining using exhaustive and simulated annealing," in *2016 Sixth International Conference on Information Science and Technology*, 2016.

[38] Y. Altintas, *Manufacturing Automation: Metal Cutting Mechanics, Machine Tool Vibrations, and CNC Design.* Cambridge University Press, 2000.

[39] M. Gen and R. Cheng, *Genetic Algorithm and Engineering Optimization.* John Wiley & Sons, 2000.

[40] Y. Wang, X. Cui, H. Xu, and K. Jiang, "Cutting force analysis in reaming of ZL102 aluminium cast alloys by PCD reamer," *International Journal of Advanced Manufacturing Technology*, vol. 67, pp. 1509–1516, 2013.

APPENDIX A

Instrument calibration

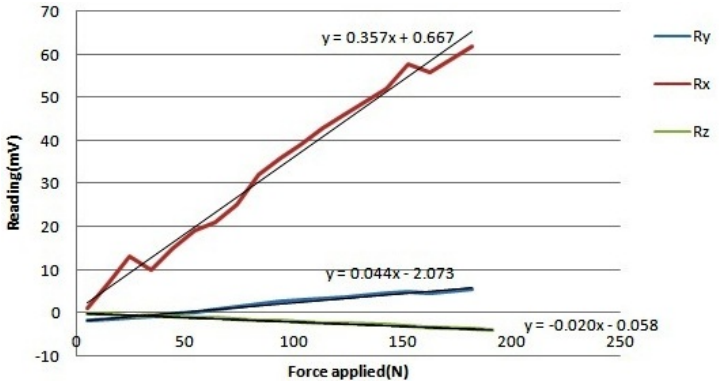

(a) Loading in x direction

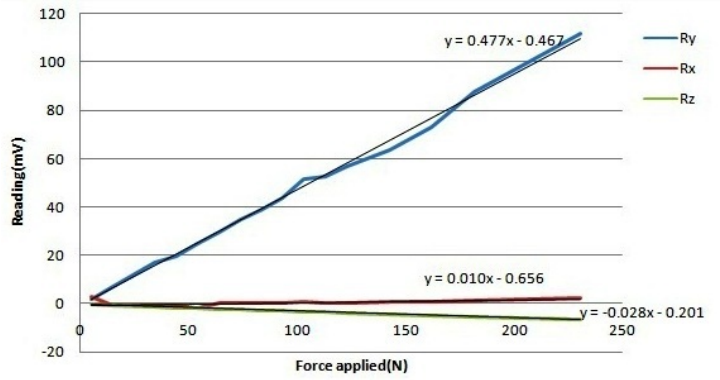

(b) Loading in y axis

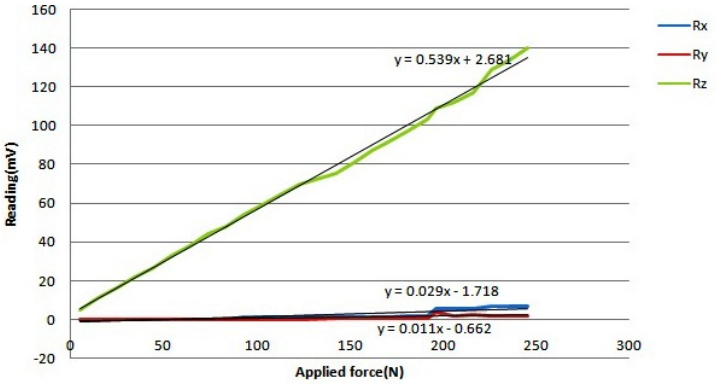

(c) Loading in z axis

Figure A.1: Dynamometer calibration curves

The set of simultaneous equations in Equation A.1 is obtained.

$$
\begin{aligned}
R_x &= 0.357 \times 10^{-}3F_x - 0.044 \times 10^{-}3F_y - 0.020 \times 10^{-}3F_z \\
R_y &= 0.477 \times 10^{-}3F_x + 0.010 \times 10^{-}3F_y - 0.028 \times 10^{-}3F_z \\
R_z &= 0.539 \times 10^{-}3F_x + 0.029 \times 10^{-}3F_y + 0.011 \times 10^{-}3F_z
\end{aligned} \tag{A.1}
$$

From this set of equations the force components in x, y and z directions are calculated using Equation A.2.

$$
\begin{aligned}
F_x &= 272.7R_x - 4.503R_y + 2.253R_z \\
F_y &= -1.411R_x + 317.5R_y + 2.691R_z \\
F_z &= -2.712R_x - 1.825R_y + 360.6R_z
\end{aligned} \tag{A.2}
$$

APPENDIX B

Matlab simulation of milling force

a=480; %(mm)axial depth

%b= %radial depth

c=0.1; %mm/tooth feedrate

omega=200; %spindle speed in Hz

n=omega*60; %spindle speed in rpm

D=8; %cutter diameter,mm

N=2; %number of teeth

beta=30; %helix angle,deg

$\text{phi}_{st} = 0; \%cutstartangle, deg$

$phi_{ex} = 180; \%cutexitangle, deg$

$\%phi =; \%referenceimmersionangle(frmbottomoffirsttooth)$

$K_{tc} = 6 * 10^8; \%tangetialcuttingcoefficient$

$K_{rc} = 1 * 10^8; \%radialcuttingcoefficient$

$K_{te} = 2 * 10^4; \%N/mm, tangetialedgecoefficient$

$K_{re} = 1 * 10^4; \%N/mm, radialedgecoefficient$

$delta_{phi} = 30; \%integrationangleof1step$

$\%delta_{phi} = 180;$

$delta_a = 48; \%lengthof1integrationstepalongaxis, mm$

$\%delta_a = 40;$

$\%\%Variables$

$phi_p = (2 * pi)/N; \%cutterpitchangle$

$K = (2 * pi)/delta_phi; \%numberofangularintegrationsteps$

$L = a/delta_a; \%numberofaxialintegrationsteps$

%

$i = 1 : K; \%integrationloop$

$phi_i = phi_st + (i * delta_phi); \%immersionangle$

$k = 1 : N; \%allteeth$

$phi_1 = phi_i + (k-1).*(phi_p); \%immersionanglefortoothk$

$phi_2 = phi_1; \%memorize$

;

$F_x(i) = 0.0;$

$F_y(i) = 0.0; \%Initializeforceintegrationsregisters$

$F_z(i) = 0.0;$

$;\ j = 1 : L; \%integratealongaxialdepth$

$a(j) = j * delta_a; \%axialposition$

$phi_2 = phi_1 - ((2 * tan(beta))/(D)) * a(j); \%updateimmersionangle$

;

$ifphi_st <= phi_2 <= phi_ex; \%cutteriscutting/immersed$

;

$h = c * sin(phi_2); \%chipthicknessatthispoint$

$deltaF_t = delta_a(K_(tc) * h + K_te); \%differentialtangential$

$deltaF_r = delta_a(K_(rc) * h + K_re); \%differentialradial$

$deltaF_x = -deltaF_t * cos(phi_2) - deltaF_r * sin(phi_2)$

$\%differentialfeed$

$deltaF_y = deltaF_t * sin(phi_2) - deltaF_r * cos(phi_2)$

$\%differentialnormal$

;

$F_x(i) = F_x(i) + deltaF_x$

$F_y(i) = F_y(i) + deltaF_y$

$F_t(i) = F_t(i) + deltaF_t$

;

$else$

$nextj;$

$nextk;$

;

$F(i) = (F_x)^(2) * (i) + (F_y)^(2) * (i)^(2); \%resultantforceatphi(i)$

$T_c(i) = (D/2) * (F_t(i)) \%cuttingtorque$

;

$nexti;$

;

$\%Plot(F_x(i), phi_i)$

$stop$

end

APPENDIX C

Flowchart of simulation

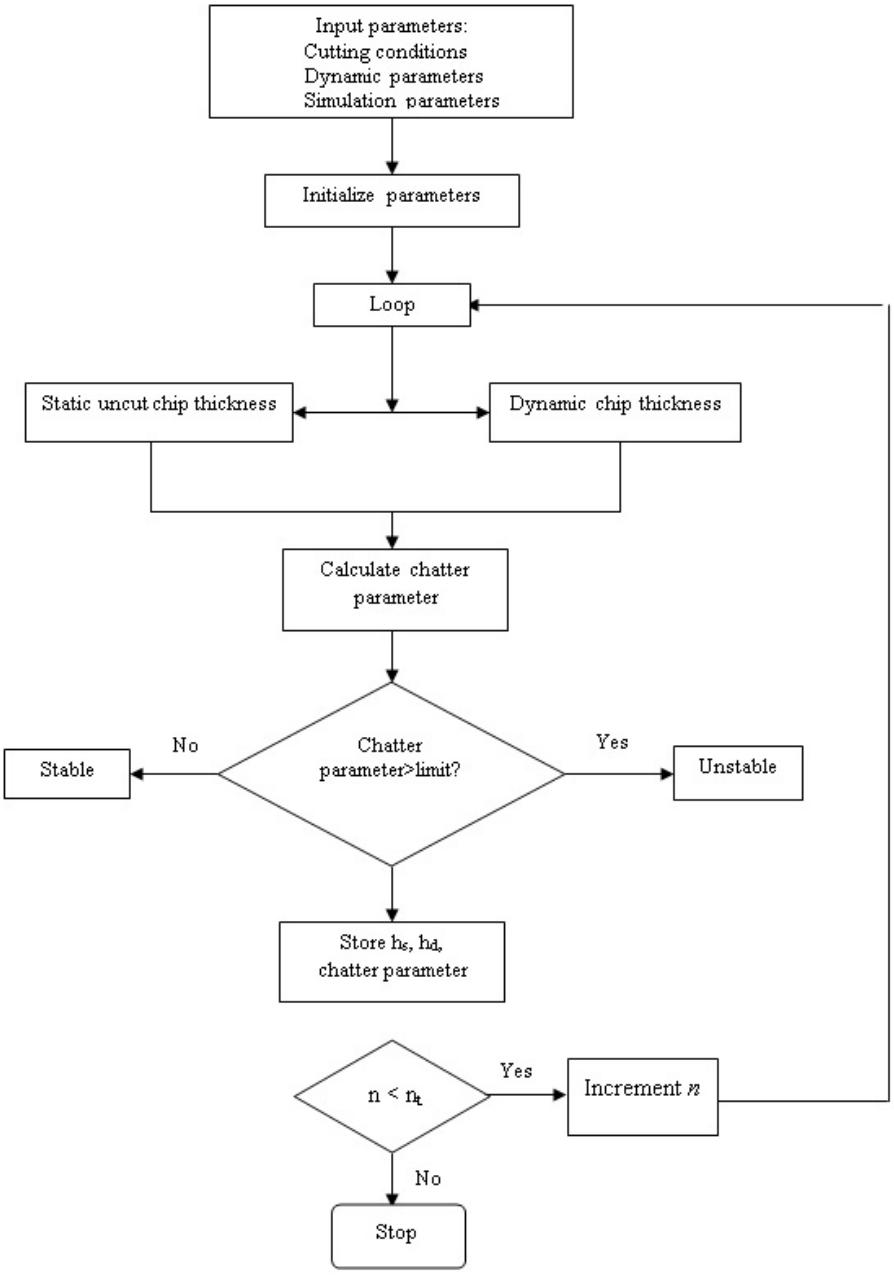

Figure C.1: Time domain simulation flowchart

APPENDIX D

Solution of dynamic equations

The dynamic milling system cannot be expressed as simple analytical functions and the dynamic differential equations which represent the system cannot be solved analytically, since the system is non-linear. Numerical methods are thus used to solve these differential equations. The solution is an approximate solution, in which the continuous time variable t is replaced by a discrete time variable, and the differential equations are solved in steps, with an increment of dt. The solution starts at known initial conditions. The solution of the Equations given in 3.8 is outlined.

The outline of how Equation3.8 was solved is as follows:

$$m_x\ddot{x} + c_x\dot{x} + k_x x = \sum_{j=0}^{N-1} F_{xj}(\phi_j) = F_x(t)$$

$$\ddot{x} = \frac{1}{m_x}(F_x(t) - k_x - c_(x)\dot{x}) \tag{D.1}$$

$$x_0 = x(0) = 0$$

$$\dot{x}_0 = x(0) = 0$$

let $x = q_1$

$\dot{x} = q_2 = \dot{q}_1$

$\ddot{x} = \dot{x}_2$

substituting this in the EquationD.1 $\dot{x} = \frac{1}{m_x}(F_x(t) - k_x q_1 - c_y x_2)$

This is solved using the MATLAB library solver ODE45, whic is based on the Runge-Kutta method, with the following syntax: ¿¿ [t,x]=ode45('myfunction',[0,0.1,5],[0,0]); ¿¿ plot(t,x)

Let $\dot{x} = p$,

$\dot{p} = f(x, p, t)$ To determine the right time steps, dt let highest natural frequency of the sytem, ω_{nmax} be given by:

$$dt \leq \frac{2\pi}{10\omega_{nmax}}$$

APPENDIX E

Labview front panels

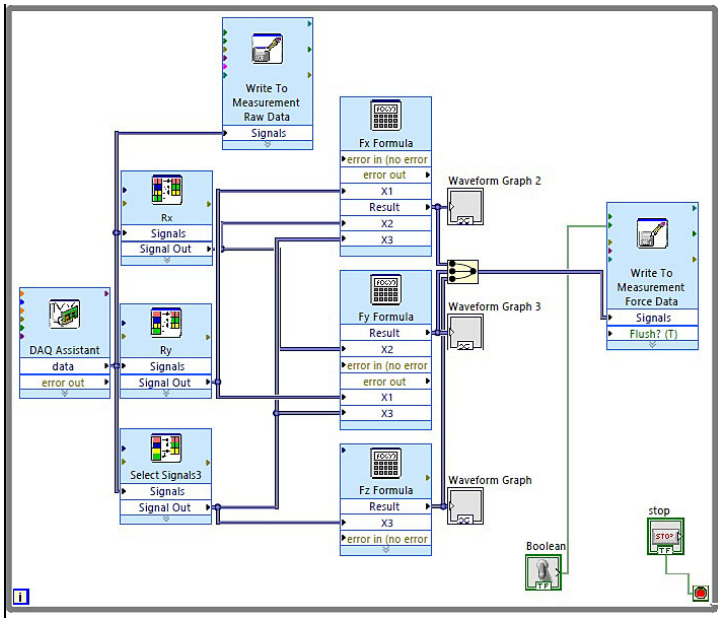

(a) Force data acquisition

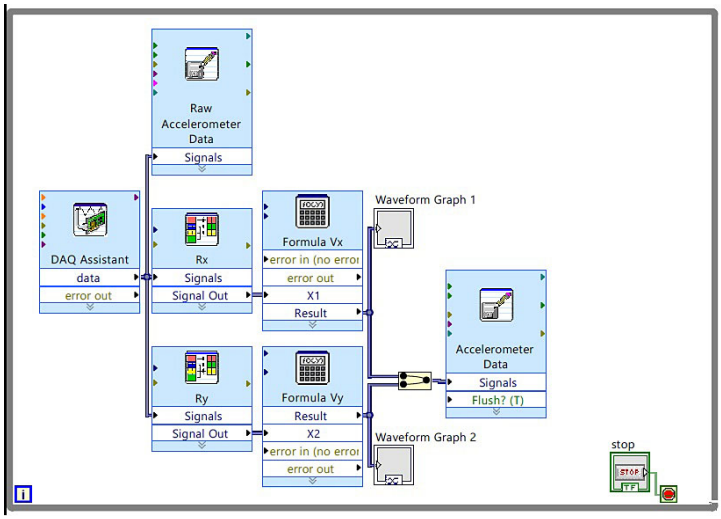

(b) Vibration data acquisition

Figure E.1: Data acquisition panels

APPENDIX F

Experimental setup

Figure F.1: Photograph of experimental setup

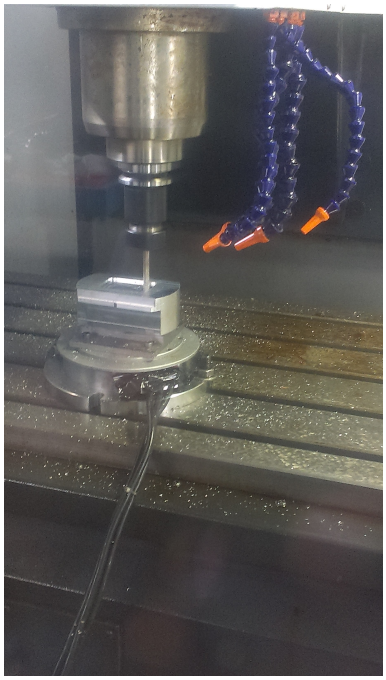

Figure F.2: Workpiece mounted on 3-axis force dynamometer

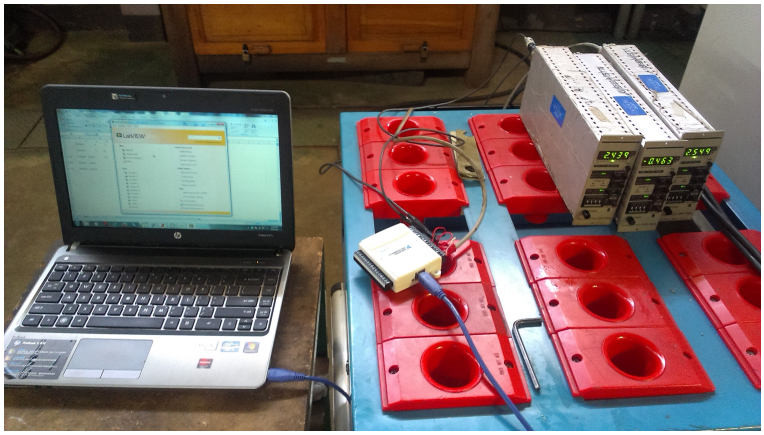

Figure F.3: Data acquisition elements

APPENDIX G

Publications

1. L. Kariuki, B. Ikua and G. Nyakoe , "Generation and Optimization of Pocket Milling Tool Paths - A Review", *Proceedings of the Sustainable Research and Innovation conference*, Vol. 5, 2014.

2. L. Kariuki, B. Ikua and G. Nyakoe, "Development of a Dynamic Cutting Force Model for Prediction of Chatter Vibration in Pocket Milling Operations", *Journal on Sustainable Research and Innovation*, vol. 3, 2016.